

KOBE-COSMO-22-12

KEK-TH-2448

KUNS-2940

Quantum current dissipation in superconducting strings and vortons

Yoshihiko Abe^{1*}, Yu Hamada^{2†}, Kota Saji^{3‡} and Koichi Yoshioka^{3§}

¹*Department of Physics, Kobe University, Kobe 657-8501, Japan*

²*KEK Theory Center, IPNS, Tsukuba, Ibaraki 305-0801, Japan*

³*Department of Physics, Kyoto University, Kyoto 606-8502, Japan*

Abstract

In this work, the current stability is discussed for cosmic strings with the bosonic superconductivity. A non-vanishing curvature of string generally induce the quantum instability of the current-carrying particle. Its decay rates are explored for various types of model parameters, curved string shapes, and decay processes. As a cosmological application, the stability is examined for superconducting strings in the string network and also for cosmic vortons by evaluating their cosmological evolution. The zero mode and hence the vorton cannot be stable in various cases, e.g., with a hierarchy between the current-carrying particle mass off the string and the string tension or with sizable couplings of the current-carrying particle to light species such as the Standard Model particles.

*yabe@diamond.kobe-u.ac.jp

†yuhamada@post.kek.jp

‡ksaji@gauge.scphys.kyoto-u.ac.jp

§yoshioka@gauge.scphys.kyoto-u.ac.jp

Contents

1	Introduction	1
2	Bosonic superconducting string	3
2.1	String and zero mode	3
2.2	Classical vorton stability	6
3	Zero mode decay	7
3.1	Lagrangian in the string background	8
3.2	Decay width	11
3.2.1	Conversion	12
3.2.2	Two-body decay	13
3.3	Square well potential	14
4	Application to cosmology	15
4.1	Parameter dependence	16
4.2	Stability of zero mode in string network	19
4.3	Vorton stability	24
5	Conclusion	29
A	Scalar Lagrangian	30
B	Propagator in the string background	31
C	Temperature dependence of Γ	34

1 Introduction

Topological defects appear in many particle physics models whose vacua have non-trivial topology. The dynamics of the defects play important roles in the history of our Universe. A well-known example is cosmic string (or vortex string) [1], which appears when a model has non-simply connected vacuum. The cosmic string has been studied for long decades as the probes of high-energy physics beyond the Standard Model (SM) of particle physics. Furthermore, it can also produce stochastic gravitational waves and is expected to be observed in the future gravitational wave detectors (e.g., Refs. [2, 3] and references therein).

Recently, current-carrying cosmic strings have gathered renewed attention. Such strings can be regarded as superconducting one-dimensional objects (if the current is

charged under the electromagnetism), and hence are called superconducting strings [4–6]. Since its existence was pointed out in [5], it has been realized that superconducting strings are ubiquitous in various extensions of the SM, e.g., the gauged $U(1)_{B-L}$ model [5, 7] and the axion models [8–13]. The current-carrying particle can be fermionic or bosonic depending on what the string couples with. The superconductivity often provides non-trivial phenomena compared to the case of conventional cosmic strings. For instance, the currents that strings carry affect their motions and make the string network dynamics different from the conventional one via the reconnection process [14–24]. The current can also affect gravitational wave spectrum from cosmic strings [25], and see also Refs. [26, 27] for the recent works. In addition, a loop of superconducting string can be a stable object, called the vorton [28, 29], which is a dark matter candidate in our Universe [30–35]. The classical stability of the vorton is understood as the balance between the centrifugal repulsive force and the attractive force associated with the string tension.

Recently, the authors of Ref. [36] discussed the instability of localized zero modes (the current-carrying particles) in superconducting strings and vortons, taking into account the effects of string bending. They studied the axion superconducting string in the KSVZ axion model [37, 38], where the zero mode comes from the KSVZ heavy quarks which are assumed to couple to the SM particles. Their conclusion is that the decay of the fermionic zero mode into light SM particles is not suppressed and that the vorton cannot be long-lived.

On the other hand, it is still unclear whether the bosonic zero mode is (un)stable in a similar fashion, while the bosonic superconductivity is realized in various models as well. In fact, some of the present authors pointed out in Ref. [12] that the axion string in the DFSZ axion model [39, 40] can be superconducting due to the zero modes consisting of the charged Higgs and W bosons in addition to fermionic carriers.¹ Since the decay phenomena of bosonic zero mode may be different from that of the fermionic one, it is necessary to clarify the charge/current stability in order to discuss the fate of superconductivity.

In this paper, we examine the (in)stability of bosonic superconductivity in the $U(1) \times \tilde{U}(1)$ model. Similarly to the result of [36], a curved string induces the decay of zero mode to the outside of the string. We calculate its decay rate for various cases of model parameters, types of curved shapes, and decay processes. As a cosmological application, we consider the string network and the cosmic vorton. It is found that the zero modes on strings and vortons are unstable in many cases. For instance, when there is a hierarchy between the mass scales of the string tension and the current-carrier particle off the string, the zero mode obtains a sufficient energy to escape from the trapping potential and easily decays. In addition, when a field producing the zero mode has sizable couplings to light particles, the corresponding decay mode is not suppressed and the superconducting

¹Similar cosmic strings appear in the two Higgs doublet model with a global $U(1)$ symmetry [41–43].

	$U(1)$ (gauge)	$\tilde{U}(1)$ (global)
Φ	0	+1
Σ	+1	0
$r \rightarrow 0$	broken	unbroken
$r \rightarrow \infty$	unbroken	broken

Table 1: The quantum charges of scalar fields and the symmetry configuration. The global $\tilde{U}(1)$ symmetry is restored at $r \rightarrow 0$ and the gauge $U(1)$ is broken around $r \sim 0$ due to the existence of string.

currents in strings and vortons do not survive to date.

The rest of the paper is organized as follows. In Section 2, the $U(1) \times \tilde{U}(1)$ model and its superconducting string solution are briefly reviewed. The classical vorton stability is also discussed. In Section 3, we derive the decay width of zero modes from curved strings and give its approximate formulae. In Section 4, we consider the zero mode decay, that is, the superconducting current dissipation in the string network and cosmic vortons, and examine whether they are stable in various parameter space. Section 5 is devoted to our conclusion. In Appendix A, we present the scalar part Lagrangian and the mass matrix for quantum fluctuations around the superconducting string background. In Appendix B, the formal scalar propagators on the background string solution are presented. The cosmological temperature dependence of the decay width is shown in Appendix C.

2 Bosonic superconducting string

In this section, we introduce the model of bosonic superconducting string with $U(1) \times \tilde{U}(1)$ symmetry, where the former $U(1)$ and latter $\tilde{U}(1)$ are gauged and global, respectively. The global $\tilde{U}(1)$ symmetry is spontaneously broken in the vacuum leading to the global string, which can be superconducting under the gauged $U(1)$ symmetry. (The gauged $\tilde{U}(1)$ case was first discussed in Ref. [5].) We also give a brief review on the classical vorton stability.

2.1 String and zero mode

The model contains two complex scalars Φ and Σ whose quantum charges are $(0, +1)$ and $(+1, 0)$ under the gauged $U(1)$ and global $\tilde{U}(1)$ symmetries, see Table 1. The Lagrangian is given by

$$\mathcal{L} = |\partial_\mu \Phi|^2 + |D_\mu \Sigma|^2 - V(\Phi, \Sigma), \quad (2.1)$$

where the covariant derivative $D_\mu = \partial_\mu - igA_\mu$ with A_μ the $U(1)$ gauge field. The scalar potential is

$$V(\Phi, \Sigma) = \frac{\lambda_\phi}{4}(|\Phi|^2 - v_\phi^2)^2 + \frac{\lambda_\sigma}{4}(|\Sigma|^2 - v_\sigma^2)^2 + \kappa|\Phi|^2|\Sigma|^2. \quad (2.2)$$

The classical equations of motion (EOMs) for the scalar fields are given by

$$\square \Phi - \frac{\lambda_\phi}{2}(v_\phi^2 - |\Phi|^2)\Phi + \kappa|\Sigma|^2\Phi = 0, \quad (2.3)$$

$$\square \Sigma - \frac{\lambda_\sigma}{2}(v_\sigma^2 - |\Sigma|^2)\Sigma + \kappa|\Phi|^2\Sigma = 0. \quad (2.4)$$

We assume that the potential has the minimum $|\Phi| = v_\phi$, $|\Sigma| = 0$ that is lower than an extremum $|\Phi| = 0$, $|\Sigma| = v_\sigma$. That implies an inequality among the couplings, $\lambda_\phi v_\phi^4 > \lambda_\sigma v_\sigma^4$. We also assume in the minimum the $U(1)$ gauge symmetry is unbroken, which means the following relation

$$m_\sigma^2 = \kappa v_\phi^2 - \frac{\lambda_\sigma}{2}v_\sigma^2 > 0, \quad (2.5)$$

where m_σ^2 is the mass-squared parameter for Σ in the vacuum. Around the vacuum expectation value v_ϕ , the radial component of Φ has the mass $m_\phi = \lambda_\phi^{1/2}v_\phi$ and the angular one is a massless Nambu-Goldstone boson. See Appendix A for the full scalar Lagrangian and the explicit form of mass matrix.

We consider a string located on the z -axes whose ansatz is

$$\Phi = \hat{\phi}(r, \theta) = v_\phi f(r) e^{i\theta}, \quad (2.6)$$

$$\Sigma = \hat{\sigma}(r, \theta) = v_\sigma h(r), \quad (2.7)$$

where r and θ are the polar coordinates transverse to the string, and $f(r)$, $h(r)$ are the profile functions satisfying the following boundary conditions

$$f(0) = 0, \quad \partial_r h(r)|_{r=0} = 0, \quad f(\infty) = 1, \quad h(\infty) = 0. \quad (2.8)$$

Substituting the ansatz (2.6) and (2.7) into the EOMs, we have

$$\frac{d^2 f}{dr^2} + \frac{1}{r} \frac{df}{dr} - \frac{1}{r^2} f + \frac{\lambda_\phi v_\phi^2}{2} (1 - f^2) f - \kappa v_\sigma^2 f h^2 = 0, \quad (2.9)$$

$$\frac{d^2 h}{dr^2} + \frac{1}{r} \frac{dh}{dr} + \frac{\lambda_\sigma v_\sigma^2}{2} (1 - h^2) h - \kappa v_\phi^2 f^2 h = 0. \quad (2.10)$$

Typical numerical solutions of these equations are shown in Fig. 1. At a large distance from the string core, $\hat{\sigma}$ goes to zero, that is, the $U(1)$ gauge symmetry is not broken. Inside the string core, $\hat{\phi}$ must vanish due to the requirement of regularity of the solution. This leads to a negative mass-squared term for Σ (see (2.2)), which triggers the condensation of

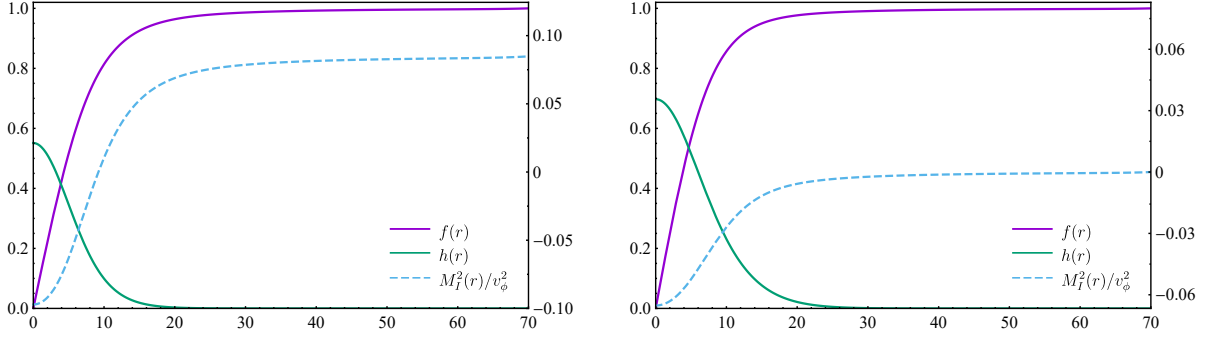


Figure 1: Typical forms of the string profile functions in the $U(1) \times \tilde{U}(1)$ model. The mass parameters are chosen as $m_\phi = m_\sigma$ (left) and $m_\phi \gg m_\sigma$ (right). The purple and green solid lines show the profiles of Φ and Σ , respectively, and their values are indicated by the left vertical axis. The blue dashed line means the position-dependent mass $M_I^2(r)$ of the imaginary part of Σ , whose values are indicated by the right vertical axis (see Section 3 for the details).

Σ inside the string. As a consequence, the $U(1)$ gauge symmetry is spontaneously broken only inside the string and it exhibits superconductivity [5].

When the magnitude of the negative mass-squared term is small, Σ does not condense to avoid a large kinetic energy. The coupling conditions for the condensation around the string is summarized [1] as

$$1 > \frac{\lambda_\sigma v_\sigma^4}{\lambda_\phi v_\phi^4} \gtrsim \frac{4\kappa}{\lambda_\sigma} > \frac{2v_\sigma^2}{v_\phi^2}. \quad (2.11)$$

We have already discussed the first and third inequalities (Eq. (2.5) and above it), the condition that at the minimum of the scalar potential, the $U(1)$ gauge symmetry is unbroken. The second inequality in (2.11) comes from the requirement for developing the condensation that the effective mass squared of Σ becomes negative around the string, whose size is roughly determined by m_ϕ . It is noted that the last requirement (the second inequality) is not necessarily needed for the condensation when the couplings satisfy a relation $m_\phi \gg m_\sigma$. In view of (2.5), the mass of Σ has two contributions to cancel and is suppressed. Such a situation can often be realized, for example, in the DFSZ axion model with a large hierarchy between the symmetry-breaking scales. On the other hand, it is easily found from (2.11) that the region $m_\phi \ll m_\sigma$ is not suitable for the condensation to occur.

It is well known that the above string solution has a $U(1)$ modulus, i.e., there is a zero mode fluctuation around the string solution. The zero mode is parametrized by the following scalar and gauge field configurations:

$$\Sigma = \hat{\sigma} e^{is(r,\theta)\eta(z,t)}, \quad (2.12)$$

$$\Phi = \hat{\phi}, \quad (2.13)$$

$$A_\mu = \frac{1}{g}\eta(z, t)\partial_\mu s(r, \theta). \quad (2.14)$$

A vanishing $s\eta$ corresponds to the string solution itself. Substituting this configuration into the EOMs, the localized mode $\eta(z, t)$ is found to obey the two-dimensional wave equation

$$(\partial_t^2 - \partial_z^2)\eta(z, t) = 0, \quad (2.15)$$

$$\left[\frac{1}{r}\partial_r(r\partial_r) + \frac{1}{r^2}\partial_\theta^2\right]s(r, \theta) = 2g^2\hat{\sigma}^2 s(r, \theta), \quad (2.16)$$

which describes the massless mode traveling along the straight string with the speed of light. This propagating mode is nothing but the charge/current carrier on the superconducting string since the $U(1)$ Noether current is written as

$$J_\mu^{U(1)} = ig\Sigma^\dagger D_\mu \Sigma + \text{h.c.} = -2\hat{\sigma}^2 s(r, \theta)\partial_\mu \eta(z, t). \quad (2.17)$$

2.2 Classical vorton stability

Let us consider a loop of superconducting string with the radius R . The scalar field characterizing the (chiral) zero mode is parametrized as

$$\hat{\sigma}(r, \theta) \exp[-i(t - z)Q/R], \quad (2.18)$$

where z is the coordinate along the string (with a periodicity $z \sim z + 2\pi R$) and Q denotes the total $U(1)$ charge on the loop. For simplicity, we here assume the zero mode on the loop is chiral, i.e., the zero mode travels only in one direction. At this stage, we do not consider any leakage of the charges and current from the string, and thus they are trapped on the loop.

Then the total energy of this loop is evaluated as

$$E_v \approx 2\pi R\mu + \frac{2\pi\mathcal{S}Q^2}{R}, \quad (2.19)$$

where μ is the string tension of the underlying vortex and $\mathcal{S} = \int d^2x \hat{\sigma}^2$, which should be $\mathcal{O}(1)$. The first term is the tension of string loop and the second one comes from the contribution of the current traveling along the loop. For the gauged $U(1)$ symmetry case, this is the Coulomb potential induced by the superconducting current. If $U(1)$ is global, this potential is regarded as a centrifugal-force potential induced by the zero mode. The energy (2.19) means that, due to the existence of current, this string loop feels a repulsion force to prevent it from shrinking. The radius of the loop is stabilized at a certain value R_0 satisfying the stationary condition $dE_v/dR = 0$, which reads

$$R_0 = Q\sqrt{\frac{\mathcal{S}}{\mu}}, \quad E_v|_{R=R_0} = 4\pi Q\sqrt{\mathcal{S}\mu}. \quad (2.20)$$

This (classically) stabilized loop of superconducting string is called the vorton [28], which behaves as a particle-like soliton with finite size R_0 . In the $(1+1)$ -dimensional sense, the zero-mode energy on the stable vorton is $Q/R = \sqrt{\mu/\mathcal{S}}$, which is typically the symmetry-breaking scale associated with the string generation.

The detailed analyses of classical vorton stability in the bosonic model are found in [44–49]. Here the vorton is considered to be classically stable as long as R_0 is much larger than the string width. On the other hand, the quantum stability has not yet established, while Ref. [28] studies a simplified calculation of the tunneling process of the zero mode. In the following, we discuss another type of quantum decay of the zero mode from string curves, which results in the current and charge dissipation from superconducting strings. This may correspond to a bosonic version of [36]. That enables us to investigate alternative quantum stability of the vorton and its cosmological application. It is the main focus of this paper.

3 Zero mode decay

We have reviewed on the superconducting string solution and the zero mode as current carrier. This is the classical solution of the EOMs containing the propagating mode on the string. In the quantum description, it is regarded as a coherent state,

$$|\text{string} + \text{zero mode}\rangle = \exp \left[i \int d^4x \left(\Sigma \Pi_\Sigma + \Phi \Pi_\Phi + A_i \Pi_A^i + \text{h.c.} \right) \right] |\text{vac}\rangle, \quad (3.1)$$

where Σ , Φ and A_i are the classical solutions describing the string and zero mode given by (2.12)–(2.14), while Π_Σ , Π_Φ and Π_A^i are the quantum operators that are canonical conjugate to Σ , Φ and A_i , respectively. Is such a state stable? In other words, can the zero mode decay into other particles? As long as a string is straight and the system on it is invariant under the straight z -direction translation, the zero mode which behaves as a massless particle in the (t, z) space, does not decay to any light particles because such a process is forbidden kinematically. However, in realistic situations such as the early Universe, strings can randomly move and hence are not generally straight. Thus the momentum along the string direction is not conserved and the decay can occur in principle. We study this type of quantum decay processes of the bosonic zero mode, i.e., the current dissipation of superconducting string in the $U(1) \times \tilde{U}(1)$ model.²

²One may wonder bosonic results should be equivalent to fermionic one [36] in view of the $(1+1)$ -dimensional duality. This is however not the case since the decay processes considered in this paper are essentially the $(3+1)$ -dimensional system.

3.1 Lagrangian in the string background

We consider the situation that a string is modified by the classical deformation $\delta\phi$ around the straight configuration $\hat{\phi}$,

$$\phi_{\text{cl}} = \hat{\phi} + \delta\phi. \quad (3.2)$$

Here and hereafter we will use barred symbols for denoting the modified string configuration. With this modification, $\hat{\sigma}$ and \hat{A}_μ should also become

$$\sigma_{\text{cl}} = \hat{\sigma} + \delta\sigma, \quad A_\mu^{\text{cl}} = \hat{A}_\mu + \delta A_\mu. \quad (3.3)$$

The induced $\delta\sigma$ and δA_μ are determined such that they satisfy the EOMs with $\delta\phi$. In this work, we suppose the weak gauge coupling limit $g \rightarrow 0$ (the so-called neutral limit). That is expected to be quantitatively justified as long as the real value of g is small [50]. Thus we hereafter drop the gauge field A_μ , which results in that the zero mode is just the Nambu-Goldstone mode of σ instead of the collective excitation (2.12) and (2.14).

The classical string deformation is parametrized as a shift into the transverse direction such that the center of straight string (on the z axis) is shifted position-dependently as $(x, y, z) = (0, \zeta(z), z)$ (Fig. 2). Then $\delta\phi$ and $\delta\sigma$, are given as

$$\delta\phi = \frac{d\hat{\phi}}{dr} \sin\theta \zeta(z), \quad \delta\sigma = \frac{d\hat{\sigma}}{dr} \sin\theta \zeta(z), \quad (3.4)$$

where $\delta\sigma$ is found from the EOMs in the first order of the string deformation. The function $\zeta(z)$ is assumed to be Fourier-expanded with the period L

$$\zeta(z) = \sum_n \zeta_n e^{-ik_n z}, \quad k_n = \frac{2\pi n}{L} \quad (n \in \mathbb{Z}), \quad (3.5)$$

with $\zeta_{-n} = \zeta_n^*$.

We study the decay process of zero modes in the background of this curved string. The quantum fluctuations of scalar fields around classical ϕ_{cl} and σ_{cl} contain the zero mode and nonzero mode particles and are expressed without bars as

$$\Phi = \phi_{\text{cl}} + \phi, \quad \Sigma = \sigma_{\text{cl}} + \sigma = \sigma_{\text{cl}} + \frac{1}{\sqrt{2}}(\sigma_R + i\sigma_I). \quad (3.6)$$

In these expressions, ϕ_{cl} and ϕ are complex, and σ_{cl} , $\sigma_{R,I}$ are real. Note that we here describe the zero mode in the linear representation for Σ instead of the nonlinear one given in (2.12) since the latter cannot be applied at infinity where $\Sigma = 0$, resulting in potential difficulties for the calculation. Both η in (2.12) and σ_I in (3.6) parametrize the Nambu-Goldstone mode on the string obeying the two-dimensional massless Klein-Gordon equation, which is regarded as the charge carrier.

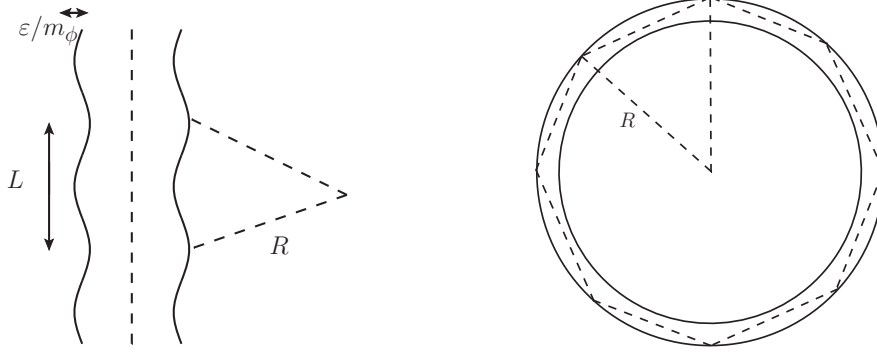


Figure 2: The schematic pictures of curved string and its loop-like object. The typical curvature radius and the period of curves are denoted by R and L .

We regard $\delta\phi$ and $\delta\sigma$ as classical but perturbative. Ignoring the interaction terms with $\delta\sigma, \delta\phi$ and other scalars, the Lagrangian for the quantum fluctuation σ_I is given by

$$\mathcal{L}_I = \frac{1}{2}(\partial_\mu \sigma_I)^2 - \frac{\lambda_\sigma}{4}(\hat{\sigma}^2 - v_\sigma^2)\sigma_I^2 - \frac{\kappa}{2}|\hat{\phi}|^2\sigma_I^2. \quad (3.7)$$

This is regarded as the free part of the Lagrangian for σ_I . Performing the mode expansion in the string background, we have

$$\sigma_I(x) = \sum_l \frac{1}{2\pi} \int \frac{d^2\mathbf{p}}{(2\pi)^2} \int \frac{d\omega^2}{2\pi} \left[a_{l,\omega^2}(\mathbf{p}) \chi_l(r, \omega^2) e^{il\theta} e^{-i\mathbf{p}\cdot\mathbf{x}} + \text{h.c.} \right]. \quad (3.8)$$

Here l denotes the angular momentum around the string and takes an integer value, and \mathbf{p} is the two-dimensional momentum in (t, z) space ($\mathbf{p}^2 = \omega^2$ if on shell). The function $\chi_l(r, \omega^2)$ is the eigenfunction of the EOM in the transverse direction

$$\left[-\frac{1}{r} \partial_r r \partial_r + \frac{l^2}{r^2} + M_I^2(r) \right] \chi_l(r, \omega^2) = \omega^2 \chi_l(r, \omega^2). \quad (3.9)$$

The position-dependent mass parameter is defined as

$$M_I^2(r) = \frac{\lambda_\sigma}{2}(\hat{\sigma}^2 - v_\sigma^2) + \kappa|\hat{\phi}|^2, \quad (3.10)$$

and is determined by the background string solution. The typical behavior of $M_I^2(r)$ are shown in Fig. 1. While the eigenvalues ω^2 are dependent on the angular momentum, we will drop the explicit index l for notational simplicity. The normalization of the eigenfunctions is

$$\int \frac{dr r}{2\pi} \chi_l(r, \omega^2) \chi_l(r, \omega'^2) = \delta(\omega^2 - \omega'^2). \quad (3.11)$$

For the discrete part of the spectrum, which we label by n , a similar normalization can be obtained by the replacement $\omega^2 \rightarrow n/L^2$ and $\delta(\omega^2 - \omega'^2) \rightarrow \delta_{nn'} L^2$. From the mode

expansion (3.8), the canonical commutation relation $[\sigma_I(t, \mathbf{x}), \dot{\sigma}_I(t, \mathbf{y})] = i\delta^3(\mathbf{x} - \mathbf{y})$ leads to the commutation relation for the creation/annihilation operator

$$[a_{l,\omega^2}(p_z), a_{l',\omega'^2}^\dagger(q_z)] = (2\pi)^3(2p^0)\delta_{l,l'}\delta(\omega^2 - \omega'^2)\delta(p_z - q_z), \quad (3.12)$$

where p^0 is the zeroth momentum component of σ_I and given by $p^0 = \sqrt{(p^z)^2 + \omega^2}$ from the on-shell condition. The total scalar Lagrangian in the modified string background is given in Appendix A including the other scalars.

The lowest mode with $l = \omega^2 = 0$, which is denoted by σ_I^0 , travels along the string with the speed of light. This is nothing but the zero mode given in Sec. 2. That is easily seen by recalling that $\hat{\sigma}$ satisfies the EOM (2.4), leading to $\chi_0(r, \omega^2 = 0) \propto \hat{\sigma}$ and

$$\hat{\sigma} + i\sigma_I^0 = \hat{\sigma} \left(1 + \frac{i}{2\pi} \int \frac{d^2\mathbf{p}}{(2\pi)^2} [a_{0,0}(\mathbf{p})e^{-i\mathbf{p}\cdot\mathbf{x}} + \text{h.c.}]_{\mathbf{p}^2=0} \right), \quad (3.13)$$

which is the zero mode (2.12) rewritten in the linear representation. The other modes with $\omega^2 \neq 0$ describe massive modes in the sense that they have the two-dimensional momentum $\mathbf{p}^2 = \omega^2 \neq 0$. The zero mode is normalizable and localized around the string with an asymptotic tail $\exp(-m_\sigma r)$. On the other hand, the massive mode with the eigenvalue ω^2 can be either normalizable or non-normalizable depending on whether ω is smaller or larger than m_σ .

The current dissipation of superconducting string is caused by the zero mode decay into non-normalizable (i.e., not localized) massive modes. As stated above, a straight string does not allow this type of decay kinematically. Therefore the curves of strings play an important role to examine the stability of superconductivity. For the perturbative analysis, the interaction terms relevant to the zero mode and first-order deformations $\mathcal{O}(\delta\phi, \delta\sigma)$ can be read off by substituting (3.6) into the Lagrangian (2.1)

$$\begin{aligned} \mathcal{L}_{\text{int}} = & -\frac{\lambda_\sigma}{2}(\hat{\sigma}\delta\sigma)\sigma_I^2 - \frac{\kappa}{2}(\hat{\phi}^*\delta\phi + \hat{\phi}\delta\phi^*)\sigma_I^2 \\ & - \frac{\lambda_\sigma}{2\sqrt{2}}(\delta\sigma)\sigma_R\sigma_I^2 - \frac{\kappa}{2}(\delta\phi^*)\phi\sigma_I^2 - \frac{\kappa}{2}(\delta\phi)\phi^*\sigma_I^2. \end{aligned} \quad (3.14)$$

The first line contains the conversion vertex between the zero mode and massive modes of σ_I . The second line is the 3-point vertices among the zero mode and other scalars. Since the zero mode is a NG boson and has odd parity associated with the CP symmetry, other vertices such as the first power of the zero mode are absent. It is noted that the vertices in the second line induce little effect on the zero mode decay. This is due to several reasons that the scalars involved are heavy far from the string, the couplings are suppressed with the string profile, and the phase space limitation. Then we are lead to studying the zero mode decay with the conversion vertices (the first line in (3.14)), which are described by the string classical deformations. Using (3.4) and (3.10), we find the conversion vertex written as

$$\mathcal{L}_{\text{int}} \supset \mathcal{L}_{\text{conv}} = \frac{1}{2}c(r, \theta, z)\sigma_I^2 \quad (3.15)$$

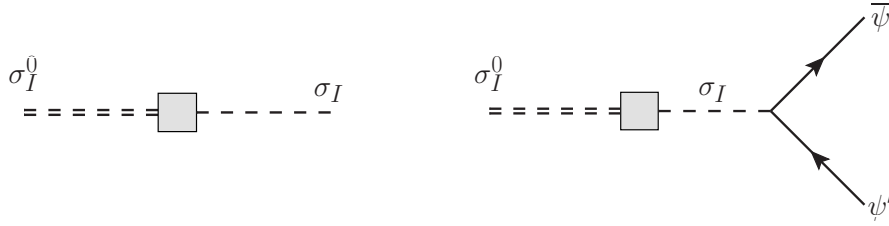


Figure 3: The zero mode decay processes. The gray box denotes the vertex from the string curve $c(r, \theta, z)$. (Left) The conversion to the bulk massive mode. (Right) The two-body decay to light modes. This process is not present in the $U(1) \times \tilde{U}(1)$ model, but naturally occurs, e.g. for the DFSZ superconducting string.

with

$$c(r, \theta, z) \equiv -\sin \theta \zeta(z) \frac{dM_I^2(r)}{dr}. \quad (3.16)$$

Within the present $U(1) \times \tilde{U}(1)$ bosonic superconductivity model, there is no effective two-body decay channel of the zero mode going out from the string due to kinematical reasons, heavy mass scales, and suppressed couplings, as stated above. On the other hand, in some extended models with the bosonic superconductivity, the current couples to light particles which gives a new decay process of the zero mode. For example, in the DFSZ axion model, the zero mode consists of the charged Higgs and W^\pm bosons and couples to the Standard Model fermion pairs due to the Yukawa couplings. To capture this aspect, let us consider the situation that a pair of bulk fermions interact to the scalar field via³

$$\mathcal{L}_\lambda = -\lambda \sigma_I \bar{\psi} \psi', \quad (3.17)$$

which generates the zero mode decay $\sigma_I^0 \rightarrow \bar{\psi} \psi'$. Here the final state fermions are assumed to be massless for simplicity.

3.2 Decay width

We evaluate the decay width of zero mode using the vertices (3.15). Let us consider two processes shown in Fig. 3: One is that the zero mode is converted to non-localized massive modes (called bulk modes) leaving from the string. The other is that the zero mode decays into a pair of light particles mediated by the bulk modes. The detail of each process will be discussed below. We assume that the total decay width is given by

$$\Gamma = \Gamma_{\text{conv}} + \Gamma_{\text{2-body}}, \quad (3.18)$$

³Such interaction may come from the Yukawa coupling of Σ and fermions with different $U(1)$ charges. The gauge anomaly is supposed to be cancelled by additional fermions with opposite charges, but its detail is qualitatively not essential to the following analysis of zero mode decay.

where Γ_{conv} and $\Gamma_{2\text{-body}}$ denote the partial decay widths of the conversion and two-body processes, respectively. Other decay processes, if any, give additive contributions to Γ .

3.2.1 Conversion

For the conversion process, consider the zero mode with the two-momentum $\mathbf{p} = (p^0, p^z) = (E, E)$ converting to the bulk mode with the four-momentum q . As stated before, this process is described by the transition from the initial state that is a coherent state including the zero mode and curved string like (3.1), into the final state consisting of bulk modes and the string deformed due to a back reaction. That requires to introduce a collective coordinate describing the string position and to quantize the collective coordinate and the zero mode simultaneously. It is however difficult to perform such a calculation particularly for the case of curved string. Therefore we take an approximation to ignore the string sector of the Hilbert space, that is, the string background is fixed throughout this process and the initial and final states are created by $a_{0,0}^\dagger(\mathbf{p})$ and $a_{l,\omega^2 \neq 0}^\dagger(\mathbf{q})$, respectively, which are the Fock space elements in the straight string background.

Thus the amplitude of the conversion process is given by

$$i\mathcal{T}_{\text{conv}} = \langle 0 | a_{l,\omega^2 \neq 0}(\mathbf{q}) \exp \left[i \int d^4x \frac{1}{2} c(r, \theta, z) \sigma_I^2(x) \right] a_{0,0}^\dagger(\mathbf{p}) | 0 \rangle \quad (3.19)$$

$$= i \int d^4x \chi_l(r, \omega^2) e^{i\mathbf{q} \cdot \mathbf{x}} e^{-il\theta} c(r, \theta, z) \chi_0(r, 0) e^{-i\mathbf{p} \cdot \mathbf{x}} \quad (3.20)$$

$$= \sum_n \zeta_n (2\pi)^2 \delta(p^0 - q^0) \delta(p^z - q^z - k_n) \int dr r \chi_0(r, 0) \chi_l(r, \omega^2) \frac{dM_I^2}{dr} \pi(\delta_{l,1} - \delta_{l,-1}), \quad (3.21)$$

where $|0\rangle$ satisfies $a_{l,\omega^2} |0\rangle = 0$. The conversion width is given by the phase space integration of the squared amplitude as

$$\Gamma_{\text{conv}} = \frac{1}{2p^0} \int \frac{dq^z d\omega^2}{(2\pi)^3 2q^0} \sum_l \frac{|\mathcal{T}_{\text{conv}}|^2}{\mathbb{T} \mathbb{L}_z} = \frac{\pi}{2E} \sum_n |\zeta_n|^2 \left| \int dr r \chi_0(r, 0) \frac{dM_I^2}{dr} \chi_1(r, \mathbf{p}_n^2) \right|^2, \quad (3.22)$$

where $\mathbf{p}_n = (p^0, p^z - k_n) = (E, E - k_n)$ and $\mathbf{p}_n^2 = 2Ek_n - k_n^2$. The system size in the time and string direction are introduced by $2\pi\delta(p^0 = 0) = \mathbb{T}$ and $2\pi\delta(p^z = 0) = \mathbb{L}_z$. Note that the z -direction momentum is not conserved because the translational invariance is violated due to the z -dependent string curves. In other words, the in-state particle obtains the momentum $-k_n$ from curves. For the zero mode to convert into bulk modes, it satisfies the kinetic condition $\mathbf{p}_n^2 \geq m_\sigma^2$ that implies the energy threshold

$$E \geq \frac{k_n^2 + m_\sigma^2}{2k_n}. \quad (3.23)$$

The sum in (3.22) is limited to the eigenstates which satisfies this bound for a fixed initial energy E .

This process seems to violate the conservation of the $U(1)$ charge defined in (2.17). The initial state has the charge $\int d^3x J_0^{U(1)} = \int dx dy \hat{\sigma}^2 E \mathbf{L}_z (\equiv Q_{init})$ while the final bulk state has the unit charge. The mismatch does not necessarily mean any inconsistency but comes from an approximation ignoring the string sector as mentioned. If one carries out the calculation within the full analysis, a back-reacted string in the final state should have explicit time dependence and carry the compensating charge $Q_{init} - 1$, and hence this process corresponds to the unit-charge leakage from the string.

3.2.2 Two-body decay

We also have the two-body decay of zero mode $\sigma_I^0 \rightarrow \bar{\psi}\psi'$ caused by the vertices $\mathcal{L}_{\text{conv}}$ and \mathcal{L}_λ . For this process, consider the zero mode with the two-momentum $\mathbf{p} = (p^0, p^z) = (E, E)$ decaying to the fermion pair with the four-momentum $q_{1,2}$. Again we make the approximation in which the string background is fixed throughout this process and the initial and final states are given by $a_{0,0}^\dagger(\mathbf{p})$ and the fermion creation operators.

The amplitude for this two-body decay is written by

$$i\mathcal{T}_{2\text{-body}} = i\lambda \int d^4x d^4x' \chi_0(r, 0) e^{-i\mathbf{p}\cdot\mathbf{x}} c(r, \theta, z) G(x, x') e^{iq_1 x'} \bar{u}(q_1) e^{iq_2 x'} v(q_2), \quad (3.24)$$

where $G(x, x')$ is the propagator for σ_I in the string background (see Appendix B for details). Its Fourier transformation with respect to the coordinates t, z, θ is

$$G(x, x') = \int \frac{d^2\mathbf{k}}{(2\pi)^3} \sum_l G_{\mathbf{k}}^l(r, r') e^{-i\mathbf{k}\cdot(\mathbf{x}-\mathbf{x}')} e^{il(\theta-\theta')}. \quad (3.25)$$

The two-body decay width is obtained by the phase space integral of this squared amplitude, exactly written as

$$\begin{aligned} \Gamma_{2\text{-body}} &= \int \frac{d^3q_1}{(2\pi)^3 2q_1^0} \frac{d^3q_2}{(2\pi)^3 2q_2^0} \frac{|\mathcal{T}_{2\text{-body}}|^2}{2p^0 \mathbf{L}_z} \\ &= \frac{|\lambda|^2}{32\pi E} \sum_n |\zeta_n|^2 \int dq^2 (\mathbf{p}_n^2 - q^2) \left| \int dr dr' r r' \chi_0(r, 0) \frac{dM_I^2(r)}{dr} G_{\mathbf{p}_n}^1(r, r') J_1(qr') \right|^2. \end{aligned} \quad (3.26)$$

$$(3.27)$$

Here J_1 is the Bessel function of first kind of order one, $2\pi J_1(r) = \int_0^{2\pi} d\theta e^{i(\theta-r\sin\theta)}$, and q means the total momentum of two fermions transverse to the string direction. We expect that the Yukawa interaction occurs essentially outside the string, and hence we take the position r' to be far from the string core. With the spectral representation of the propagator

$$G_{\mathbf{k}}^l(r, r') = \int \frac{d\omega^2}{2\pi} \frac{1}{\omega^2 - \mathbf{k}^2} \chi_l(r, \omega^2) \chi_l(r', \omega^2), \quad (3.28)$$

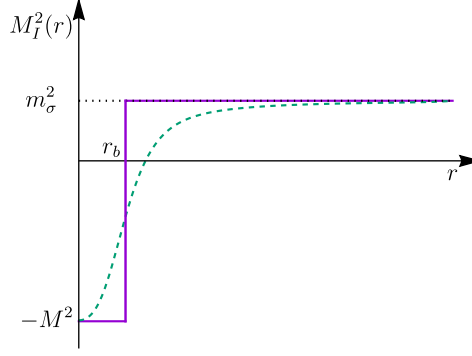


Figure 4: The schematic picture of square well potential as an approximation of the position-dependent mass function $M_I^2(r)$.

and the asymptotic form $\chi_1(r', \omega^2) \sim \pi^{1/2} J_1(\sqrt{\omega^2 - m_\sigma^2} r')$, we obtain the decay width as

$$\Gamma_{2\text{-body}} \approx \frac{|\lambda|^2}{32\pi E} \sum_n |\zeta_n|^2 \int d\omega^2 \frac{\mathbf{p}_n^2 - \omega^2 + m_\sigma^2}{(\omega^2 - \mathbf{p}_n^2)^2} \left| \int dr r \chi_0(r, 0) \frac{dM_I^2(r)}{dr} \chi_1(r, \omega^2) \right|^2, \quad (3.29)$$

Once the couplings in the model are fixed, the eigenfunctions and mass parameters are determined and then the decay widths are evaluated using (3.22) and (3.29).

In the case that the energy threshold condition (3.23) is met, for example, by a large initial energy of the zero mode, the intermediate state can be on shell at specific values of ω (the poles of the propagator $G_{\mathbf{p}_n}^1$). The on-shell decay width may be evaluated by a replacement

$$\frac{1}{(\omega^2 - \mathbf{p}_n^2)^2} \rightarrow \frac{1}{(\omega^2 - \mathbf{p}_n^2)^2 + \omega^2 \Gamma_\omega^2}. \quad (3.30)$$

Here we assume that the width is given by $\Gamma_\omega = |\lambda|^2 m_\sigma / 8\pi$ as the bulk mode mass in four-dimensional viewpoint is approximated by m_σ outside the string.

3.3 Square well potential

Some analytical expressions for the partial decay widths can be obtained by the approximation that the position-dependent mass function $M_I^2(r)$ is regarded as a squared well potential shown in Fig. 4:

$$M_I^2(r) = -M^2 \theta(r_b - r) + m_\sigma^2 \theta(r - r_b), \quad (3.31)$$

where $\theta(r)$ is the Heaviside step function. The parameters M^2 and r_b represent the depth and width of the well potential, respectively, and we have

$$M^2 \sim \lambda_\sigma v_\sigma^2, \quad r_b = m_\phi^{-1}, \quad (3.32)$$

which are typically expected from the form of string solution discussed in the previous section. The asymptotic value m_σ^2 is the mass of σ at large distance from the string and is defined in (2.5).

In this approximation, the eigenfunctions are explicitly given by the (modified) Bessel functions as $\chi_0(r, 0) \sim \sqrt{4\pi} m_\sigma K_0(m_\sigma r)$ and $\chi_1(r, \omega^2) \sim \sqrt{\pi} J_1(\sqrt{\omega^2 - m_\sigma^2} r)$ for $r \geq r_b$, and the integrals in (3.22) and (3.29) can be performed. That leads to the analytic formulae

$$\Gamma_{\text{conv}} \approx \frac{2\pi^3}{E} (M^2 + m_\sigma^2)^2 (m_\sigma r_b)^2 K_0(m_\sigma r_b)^2 \sum_n |\zeta_n|^2 J_1(\sqrt{\mathbf{p}_n^2 - m_\sigma^2} r_b)^2, \quad (3.33)$$

$$\begin{aligned} \Gamma_{\text{2-body}} \approx & \frac{\pi |\lambda|^2}{8E} (M^2 + m_\sigma^2)^2 (m_\sigma r_b)^2 K_0(m_\sigma r_b)^2 \sum_n |\zeta_n|^2 \\ & \times \int_{m_\sigma^2}^{m_\sigma^2 + \mathbf{p}_n^2} d\omega^2 \frac{\mathbf{p}_n^2 - \omega^2 + m_\sigma^2}{(\omega^2 - \mathbf{p}_n^2)^2} J_1(\sqrt{\omega^2 - m_\sigma^2} r_b)^2. \end{aligned} \quad (3.34)$$

Here K_0 is the modified Bessel function of second kind. These expressions are useful for discussing the cosmological consequences of superconducting strings and the zero mode behavior in the next section.

4 Application to cosmology

As an application of the zero mode decay processes in the previous section, we examine the stability of superconducting strings and vortons against the string curves.

Instead of specifying the couplings in the Lagrangian, we replace them with the mass scale parameters defined as

$$m_\sigma^2 = \kappa v_\phi^2 - \frac{\lambda_\sigma}{2} v_\sigma^2, \quad m_\phi^2 = \lambda_\phi v_\phi^2, \quad M^2 = \frac{1}{2} \lambda_\sigma v_\sigma^2. \quad (4.1)$$

The physical meanings of these mass parameters are as follows: m_σ determines the tail behavior of zero mode wavefunction (the mass of σ far from the string), m_ϕ represents the width of string, and M means the depth of the well potential that the zero mode feels. With the coupling conditions for superconductivity (2.11), we find $m_\sigma^2 > 0$ and $M^4 \gtrsim m_\phi^2 (M^2 + m_\sigma^2)$, which necessarily implies $M \gtrsim m_\phi$. In addition, unless no huge hierarchy exists among the dimensionless couplings, (2.11) also implies $M \lesssim m_\phi$. These fact leads us to a reasonable assumption $M = m_\phi$, which then means $m_\phi \gtrsim m_\sigma$ from (2.11). In the following analysis, we thus assume

$$m_\sigma < m_\phi = M \quad (4.2)$$

for the parameter region preferable for the superconductivity. As for the magnitude of m_σ , we have checked any desired (small) value can be realized by appropriately choosing the coupling constants under the conditions of superconductivity.

The curved string is generally possible to take various forms expressed by the function $\zeta(z)$, whose Fourier expansion is given in (3.5). In the following analysis, we implicitly consider the $n = 1$ mode only. The contributions from other modes with $n > 1$ can be evaluated by taking the n dependence of k_n into account. In general, the energy condition like (3.23) leads to an upper bound on n , and the dominant effect usually comes from a smaller n unless the string curve is singular. We denote the width of this mode as

$$|\zeta_1| = \frac{\varepsilon}{m_\phi}, \quad (4.3)$$

where ε is the relative size of curve compared to the string width and should be smaller than unity for the perturbative analysis to be valid. The width of curve is also rewritten by using the curvature radius R (see Fig. 2) in the large radius limit,

$$\frac{\varepsilon}{m_\phi} \approx \frac{L^2}{4\pi^2 R}. \quad (4.4)$$

If a cosmic string is present in the early Universe at the temperature T , a typical size of its curvature radius is given by the inverse of the Hubble parameter $H(T)$ (assuming the scaling regime). From the Friedmann equation in the radiation dominated era, we have

$$H(T) = \sqrt{\frac{\pi^2 g_*}{90}} \frac{T^2}{M_P}, \quad (4.5)$$

where $M_P = 2.44 \times 10^{18}$ GeV is the reduced Planck scale and g_* the effective degrees of freedom for the energy density at T . We here assume for simplicity that g_* is a constant of order 10^2 .

4.1 Parameter dependence

Before discussing the cosmological implications, we illustrate the parameter dependence of the zero mode decay width. As a benchmark case, we fix the curvature radius by the Hubble parameters, $R = H(T)^{-1}$. The typical length of L is also fixed by the relation (4.4). We then have three parameters in addition to the mass scale parameters m_σ and m_ϕ : the initial energy E of zero mode, the curve size ε , and the Yukawa coupling λ for the two-body decay.

E dependence : First we examine the energy E dependence. In Fig. 5, the partial decay widths Γ_{conv} and $\Gamma_{\text{2-body}}$ are shown by the solid and dotted lines, respectively. We here show two typical cases that the mass scales inside and outside the string are of the same order $m_\phi = m_\sigma$ (left panel) and hierarchical $m_\phi \gg m_\sigma$ (right panel). The energy dependence is found to be classified into four regions: (i) $E \lesssim k_n$, (ii) $k_n \lesssim E \lesssim m_\sigma^2/k_n$, (iii) $m_\sigma^2/k_n \lesssim E \lesssim m_\phi^2/k_n$, and (iv) $m_\phi^2/k_n \lesssim E$ in the case $m_\sigma > k_n$, which is possible if the mass scales satisfy $m_\phi M^2 \lesssim \varepsilon m_\sigma^2 M_P$. For $m_\sigma < k_n$, a similar classification appears by exchanging m_σ^2/k_n and k_n , and then the region (ii) almost vanishes.

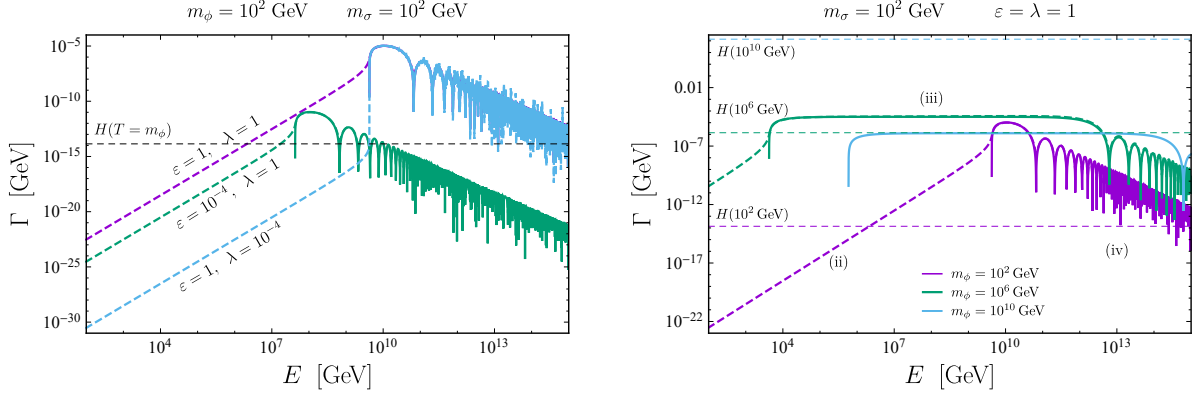


Figure 5: The initial energy dependence of the zero mode decay width at the temperature $T = m_\phi$ with various parameter sets. (Left) The purple, green, blue lines correspond to the parameters $(\varepsilon, \lambda) = (1, 1)$, $(10^{-4}, 1)$, and $(1, 10^{-4})$, respectively. The solid and dotted parts mean Γ_{conv} and $\Gamma_{2\text{-body}}$ (the purple-solid and blue-solid lines are overlapped). The mass parameters are fixed $m_\phi = m_\sigma = 10^2$ GeV. (Right) The purple, green, blue lines correspond to $m_\phi = 10^2, 10^6$ and 10^{10} GeV, while m_σ is 10^2 GeV. The other couplings are fixed as $\varepsilon = \lambda = 1$. In both figures, the horizontal dashed lines show the Hubble parameter at $T = m_\phi$. The regions (ii), (iii), (iv) imply the classification of the energy dependence of the width. See the text for details.

- Region (i) : Any decay is forbidden kinematically.

In the words of the 2-dimensional transverse momentum $\mathbf{p}_n = (E, E - k_n)$, this region means $\mathbf{p}_n^2 < 0$. Due to a relatively large size of curve, the final (total) momentum becomes tachyonic.

- Region (ii) : Only the two-body decay is possible.

In this region, $\mathbf{p}_n^2 < m_\sigma^2$ and the energy threshold (3.23) is not met. Therefore only a decay to lighter modes (than m_σ) can occur. With the series expansion for the Bessel functions, the width of zero mode is found to have the parameter dependence

$$\Gamma \propto \varepsilon^{1/2} \lambda^2 E^2 M^7 / (m_\phi^{9/2} m_\sigma^2), \quad (4.6)$$

and increases as the energy E (the dotted lines in the figures). It weakly depends on the curve size ε . Later, we will consider the case $E = m_\phi$ for superconducting current, which belongs to this region (ii) if $m_\phi^3 M^2 \lesssim \varepsilon m_\sigma^4 M_P$.

- Region (iii) : Both the conversion and two-body decay are possible.

The energy threshold condition is satisfied and $\mathbf{p}_n^2 > m_\sigma^2$. The two-body decay is dominated by the poles of the propagator (in the string background) as long as the width is perturbatively narrow. The zero mode decay width is roughly given by

$$\Gamma \propto \varepsilon^{3/2} M^5 m_\sigma^2 / m_\phi^{11/2}. \quad (4.7)$$

This is free from λ as it should be. Further Γ is a constant against the initial energy E (the plateau seen in the right panel). The plateau generally appears when the region (iii) is effective, i.e., $m_\sigma < m_\phi$. For the hierarchical mass case $m_\sigma \ll m_\phi$, the height of plateau is proportional to $m_\sigma^2/m_\phi^{1/2}$ and the decay width becomes small. The case $E = m_\phi$ for superconducting current belongs to this region (iii) if $m_\phi^3 M^2 \gtrsim \varepsilon m_\sigma^4 M_P$.

- Region (iv) : All the decay widths are suppressed.

In this region, the transverse momentum of final states is $\mathbf{p}_n^2 > m_\phi^2$. For such higher energy in the radial direction, their Compton wavelengths become shorter than the string width, and hence the overlapping integral of wavefunctions in Γ is oscillationally suppressed.⁴ The decay width decreases with energy as

$$\Gamma \propto \varepsilon^{9/4} M^{7/2} m_\sigma^2 / (E^{3/2} m_\phi^{13/4}). \quad (4.8)$$

The energy threshold (3.23) for the conversion and on-shell decay corresponds to the boundary between the solid and dotted lines in Fig. 5. It has the complex dependence on mass parameters. For a smaller value of m_ϕ , that is, $m_\phi < \varepsilon m_\sigma^2 M_P / M^2$, the threshold scale is $\varepsilon^{1/2} m_\sigma^2 M_P^{1/2} / M m_\phi^{1/2}$ (a decreasing function of m_ϕ). For larger m_ϕ , it is $M m_\phi^{1/2} / \varepsilon^{1/2} M_P^{1/2}$ (increasing with m_ϕ). Therefore the threshold energy has the minimum around $m_\phi \sim \varepsilon m_\sigma^2 M_P / M^2$. For a larger m_ϕ than this minimum, the off-shell two-body decay becomes almost ineffective (see the blue line in the right panel). Above the threshold, the conversion and on-shell decay processes open up. That is possible for the zero mode with $E = m_\phi$ only when m_ϕ is larger than $(\varepsilon m_\sigma^4 M_P / M^2)^{1/3}$.

ε, λ dependence : Next we show the coupling ε, λ dependence. Fig. 6 is the contour plot of the decay width Γ over the Hubble parameter H . The left panel is for the curve size ε and the right one for the Yukawa coupling λ to light fermions. In the region $\Gamma > H$ (the shaded region), the zero mode immediately decays in the early Universe and the superconducting current is unstable. The initial energy and the temperature are fixed at $E = T = m_\phi$ in the figure. In the blue region, the threshold condition (3.23) is satisfied and the conversion (on-shell decay) is possible. On the other hand, in the green region, only the two-body decay via off-shell mediator is allowed. The boundary of these two colored regions is given by the equation $m_\phi M^2 = \varepsilon m_\sigma^2 M_P$ as noted above, which is independent of λ .

From the left panel of Fig. 6, one can see that the decay width tends to decrease for a smaller size of string curve. In the straight string limit, the superconducting current becomes stable [36]. Around the right-lower corner where ε is small and m_ϕ is large,

⁴In the framework with the momentum conservation, an alternative view of this suppression is obtained from the dynamics of Nambu-Goldstone boson [51, 52] appearing as a result of the translation symmetry breaking due to the presence of string.

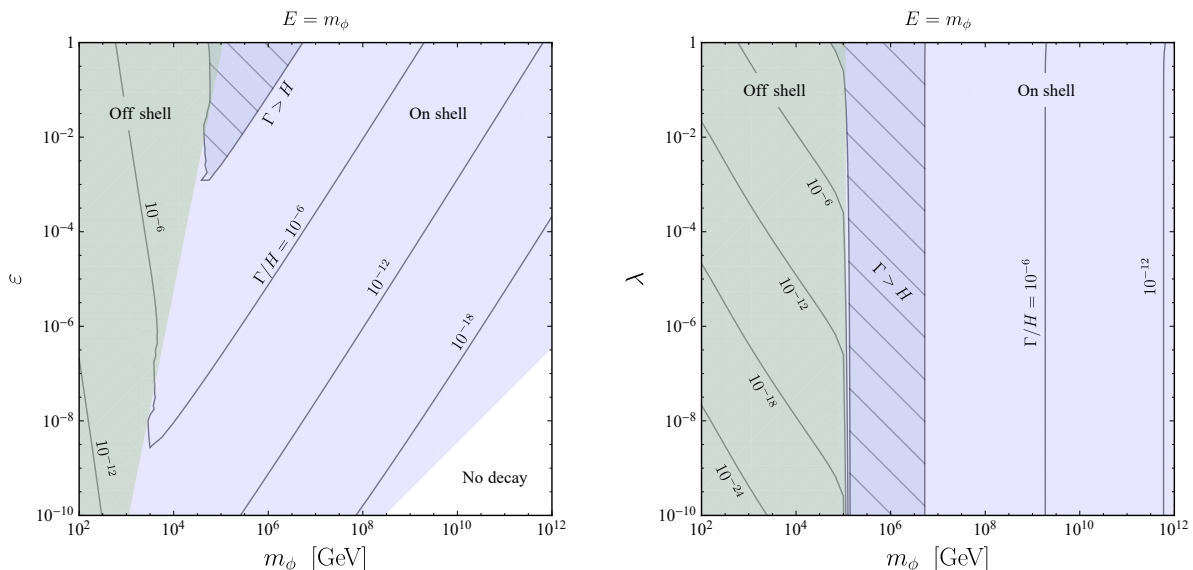


Figure 6: The coupling dependence of the zero mode decay width. The blue (“on shell”) region means the initial energy is above the threshold. In the green (“off shell”) region, only the two-body decay is possible. The on-shell decay width does not depend on λ as it should be. For the “no decay” region, see the text for detail.

$k_n \propto (m_\phi/\varepsilon)^{1/2}$ becomes large and then $\mathbf{p}_n^2 < 0$. Therefore any decay process is forbidden there.

The Yukawa coupling dependence is read from the right panel of Fig. 6. For a smaller coupling, the two-body decay decreases but the conversion does not. In the tiny coupling limit, only the on-shell decay process is valid. We will discuss in the following analysis the two distinct cases: (i) both of the decay processes are possible and (ii) only the conversion is included. When the two-body decay process is effective, we will set $\lambda = 1$ as a benchmark value.

4.2 Stability of zero mode in string network

In the early Universe, conventional cosmic strings without superconductivity are considered to form a network and obey the scaling behavior thanks to the reconnection process. We now discuss whether the zero modes on superconducting strings can affect the dynamics of its network. In order to affect the string dynamics, the current that the zero modes carry should be comparable to the mass scale of the string tension, $\sqrt{\mu} \sim m_\phi$, and hence the zero mode should have an energy of the order of m_ϕ since the amount of the current is roughly estimated as $\sim E$. Thus we study the stability of the zero mode with the energy $E = m_\phi$ in the string network. In general, the current on the string is not chiral but a superposition of chiral zero modes in the string network. For instance, a

superconducting string moving in the magnetic field background gets a current without charges [5, 6], which is described by a superposition of the chiral zero modes traveling in the opposite directions. While such a case admits yet another channel for the current dissipation given by the collision of zero modes, we do not consider this type of process focusing the decay of single chiral zero mode.

In the analysis below, any generation process of the superconducting current is not needed to be specified. Whether a sufficient current can be generated depends on the time evolution of strings (and other background fields). Further, we focus on the stability of zero modes and assume that the dynamics of string network is approximately given by the conventional scaling solution. If zero modes are sufficiently stable, one may need to solve the coupled equations describing the dynamics both of the string network and the zero mode current in terms of, e.g., the velocity-dependent one-scale (VOS) model for current-carrying strings [23, 24, 26].

In the present case, there are two types of string curves. First, in the scaling regime, strings have one typical macroscopic length scale which is comparable to the Hubble length. Thus the curvature radius and the period of curves are considered as the Hubble length, $R \sim L \sim H(T)^{-1}$. For such a macroscopic curve, the perturbative analysis generally breaks down. We therefore fix $R = H(T)^{-1}$ and take L such that $\varepsilon = 1$. That may give an approximate lower bound of the decay rate in the string network. Secondly, strings can receive an energy from thermal plasma (if they interact with plasma particles) which gives microscopic random curves of strings. This thermal curve is roughly given by $\delta\phi \sim T \sin(Tz)$ where the typical momentum scale is $\mathcal{O}(T)$. That corresponds to the function

$$\zeta(z) \sim \frac{T}{m_\phi v_\phi} \sin(Tz). \quad (4.9)$$

In order for the perturbative analysis to be valid, the thermal contribution should satisfy $L \gg 1/m_\phi$ and $\epsilon \sim T/v_\phi \lesssim 1$, leading to

$$T \ll m_\phi, \quad (4.10)$$

which is achieved by taking into account the thermal curves only when $T < 10^{-3}m_\phi$. In the following, we evaluate the decay width for each type of curves separately. That is justified at the leading order of perturbations.

These two types of string curves give different temperature dependence of the zero mode decay width. We show them in Fig. 7 for a benchmark point where $E = m_\phi$ and $m_\sigma = 10^2$ GeV. The left and right panels correspond to the curve with $R = H^{-1}$ and the thermal one, respectively. In the left panel, one can see that the behavior of Γ changes at the transition temperature $T_{\text{trs}}^{\text{Hub}} \sim m_\sigma^2 M_P^{1/2} / m_\phi^{3/2}$. The asymptotic behaviors at high and low temperatures can be seen by substituting R and L into the approximate formulae (3.33) and (3.34). In the high temperature region, two partial decay widths Γ_{conv} and

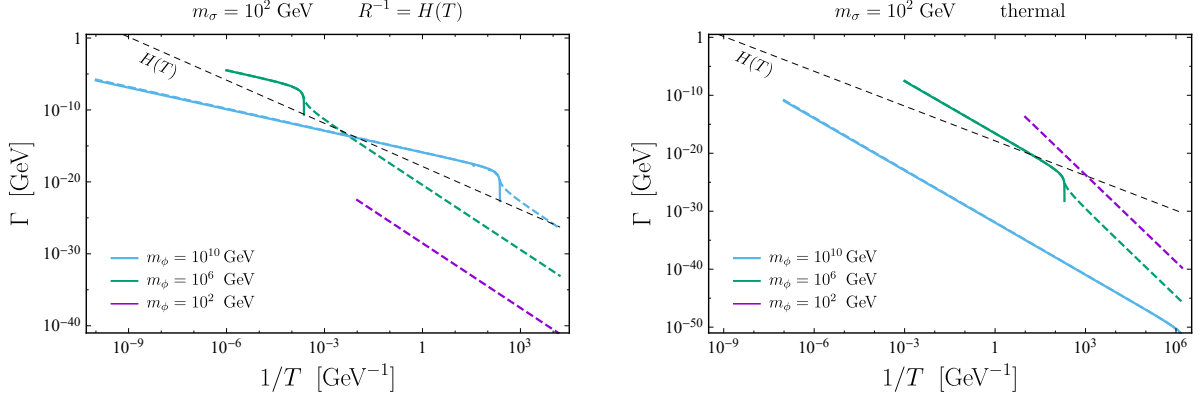


Figure 7: The temperature dependence of the zero mode decay width with $E = m_\phi$ and $m_\sigma = 10^2$ GeV. The colored solid and dashed lines correspond to the conversion Γ_{conv} and the two-body decay $\Gamma_{2\text{-body}}$, respectively. (Some dashed and solid lines are overlapped.) The dashed black lines denote the Hubble parameter $H(T)$. (Left) The dependence comes from $R = H^{-1}$ (the scaling regime). The Yukawa coupling is set to $\lambda = 1$. (Right) The thermal curve with which the analysis is assumed to be valid at $T < 10^{-3}m_\phi$.

$\Gamma_{2\text{-body}}$ agree since the latter is dominated by the on-shell production of massive modes, and they become

$$\Gamma_{\text{conv}}^{\text{Hub}} \approx \Gamma_{2\text{-body}}^{\text{Hub}} \approx T \frac{m_\sigma^2}{m_\phi^{3/2} M_P^{1/2}} \left[\log \left(\frac{m_\sigma}{m_\phi} \right) \right]^2 \quad \text{for } T \gtrsim T_{\text{trs}}^{\text{Hub}}, \quad (4.11)$$

where we have used the series expansions for the Bessel functions $J_1(x) \sim x$ and $K_0(x) \sim (\log x)^2$, dropping $\mathcal{O}(1)$ numerical coefficients. In the low temperature region, the on-shell production is kinematically forbidden and hence only the two-body decay $\Gamma_{2\text{-body}}$ is nonzero, leading to

$$\Gamma_{\text{conv}}^{\text{Hub}} = 0, \quad \Gamma_{2\text{-body}}^{\text{Hub}} \approx T^3 \frac{\lambda^2 m_\phi^{3/2}}{m_\sigma^2 M_P^{3/2}} \left[\log \left(\frac{m_\sigma}{m_\phi} \right) \right]^2 \quad \text{for } T \lesssim T_{\text{trs}}^{\text{Hub}}. \quad (4.12)$$

For the thermal curves (the right panel in Fig. 7), the behavior of Γ changes at $T_{\text{trs}}^{\text{th}} \sim m_\sigma^2/m_\phi$. The asymptotic behaviors are obtained in a similar way as above. The decay width via the thermal curve is evaluated by substituting (4.9) into (3.33) and (3.34). In the high temperature region, two partial decay widths Γ_{conv} and $\Gamma_{2\text{-body}}$ also agree and are given by

$$\Gamma_{\text{conv}}^{\text{th}} \approx \Gamma_{2\text{-body}}^{\text{th}} \approx T^3 \frac{m_\sigma^2}{m_\phi^4} \left[\log \left(\frac{m_\sigma}{m_\phi} \right) \right]^2 \quad \text{for } T \gtrsim T_{\text{trs}}^{\text{th}}, \quad (4.13)$$

while in the low temperature region, only the latter is non-vanishing

$$\Gamma_{\text{conv}}^{\text{th}} = 0, \quad \Gamma_{2\text{-body}}^{\text{th}} \approx T^5 \frac{\lambda^2}{m_\sigma^2 m_\phi^2} \left[\log \left(\frac{m_\sigma}{m_\phi} \right) \right]^2 \quad \text{for } T \lesssim T_{\text{trs}}^{\text{th}}. \quad (4.14)$$

(The above expressions are numerically confirmed in Appendix C.) Note that in both temperature regions the decay widths via the thermal curves have steeper slopes with respect to $1/T$ than that of the Hubble parameter. Therefore in the case of thermal curve the stability of zero mode is determined at higher temperature, which means the ratio Γ/H is “ultraviolet (UV)-dominated”.

It may be worthwhile commenting on how the decay width depends on m_ϕ . At first, the partial widths Γ_{conv} and $\Gamma_{\text{2-body}}$ contain several parts $(M^2 + m_\sigma)^2$, r_b^2 , and $J_1(\sqrt{\mathbf{p}_n^2 - m_\sigma^2} r_b)^2$ (or $J_1(\sqrt{\omega^2 - m_\sigma^2} r_b)^2$), each of which comes from the potential depth, the r -integration measure, and the wavefunction of the bulk mode χ_1 , giving the dependence m_ϕ^4 , m_ϕ^{-2} , and $\mathbf{p}_n^2 m_\phi^{-2}$, respectively, for $m_\phi \gg m_\sigma$. The reason why the last one is inversely proportional to m_ϕ is that larger m_ϕ (smaller r_b) reduces the overlap between the zero mode and the bulk mode wavefunctions. Thus the dependence from the potential shape disappears and the widths become $\Gamma_{\text{conv}} \propto |\zeta_n|^2 \mathbf{p}_n^2 / E \approx \epsilon^2 k_1 / m_\phi^2$ and $\Gamma_{\text{2-body}} \propto |\zeta_n|^2 \mathbf{p}_n^6 / E \approx \epsilon^2 E^2 k_1^3 / m_\phi^2$, where we have dropped m_σ and assumed the off-shell contribution from the bulk modes for $\Gamma_{\text{2-body}}$, leading to the suppression of $\Gamma_{\text{2-body}}$ for smaller E and k_1 . From these expressions, we can intuitively state that the decay widths are reduced for larger m_ϕ with fixed E , k_1 and ϵ because the string becomes too heavy to be deformed. If one sets $E = m_\phi$, however, a more careful treatment is needed particularly for $\Gamma_{\text{2-body}}$. Indeed, by taking $E = m_\phi$, the explicit m_ϕ -dependence is canceled and the dependence comes only through ϵ and k_1 , which may give positive powers of m_ϕ depending on the types of string curves. This is why $\Gamma_{\text{2-body}}$ contains the positive power as $m_\phi^{3/2}$ in Eq. (4.12).

Now, we present the parameter space in which the zero mode affect the string dynamics. We consider the both types of string curves. At a temperature T , the zero mode immediately decays if $\Gamma(T) > H(T)$ holds, resulting in the usual string network without any significant current. We also assume that the current and charge are not supplied after the decay.

In Fig. 8, we show such a parameter space on the (m_ϕ, m_σ) -plane with the $\Gamma(T)$ behavior. Only the conversion process is taken into account in the top two panels while both processes are in the bottom two panels. The left two panels correspond to the curve with $R = H^{-1}$ while the right two panels to the thermal one. The colored region in the left panels show the parameter space for m_σ and m_ϕ in which the zero mode decay becomes significant, i.e., $\Gamma(T) > H(T)$ holds at some stage in the Universe. The contours correspond to when a transition from $\Gamma(T) < H(T)$ to $\Gamma(T) > H(T)$ occurs, i.e., the temperature T_{eq} such that $\Gamma(T_{\text{eq}}) = H(T_{\text{eq}})$. The blue regions represent that $\Gamma(T) > H(T)$ is already met at $T = m_\phi$, i.e., at the stage of the production of strings. The white blank represents the parameter space in which the zero mode survives at all stages, i.e., $\Gamma(T) < H(T)$ for arbitrary T . “No decay” in the white blank indicates that the decay cannot occur kinematically since the threshold condition (3.23) cannot be satisfied there, while “No dissipation” indicates that the decay can occur kinematically

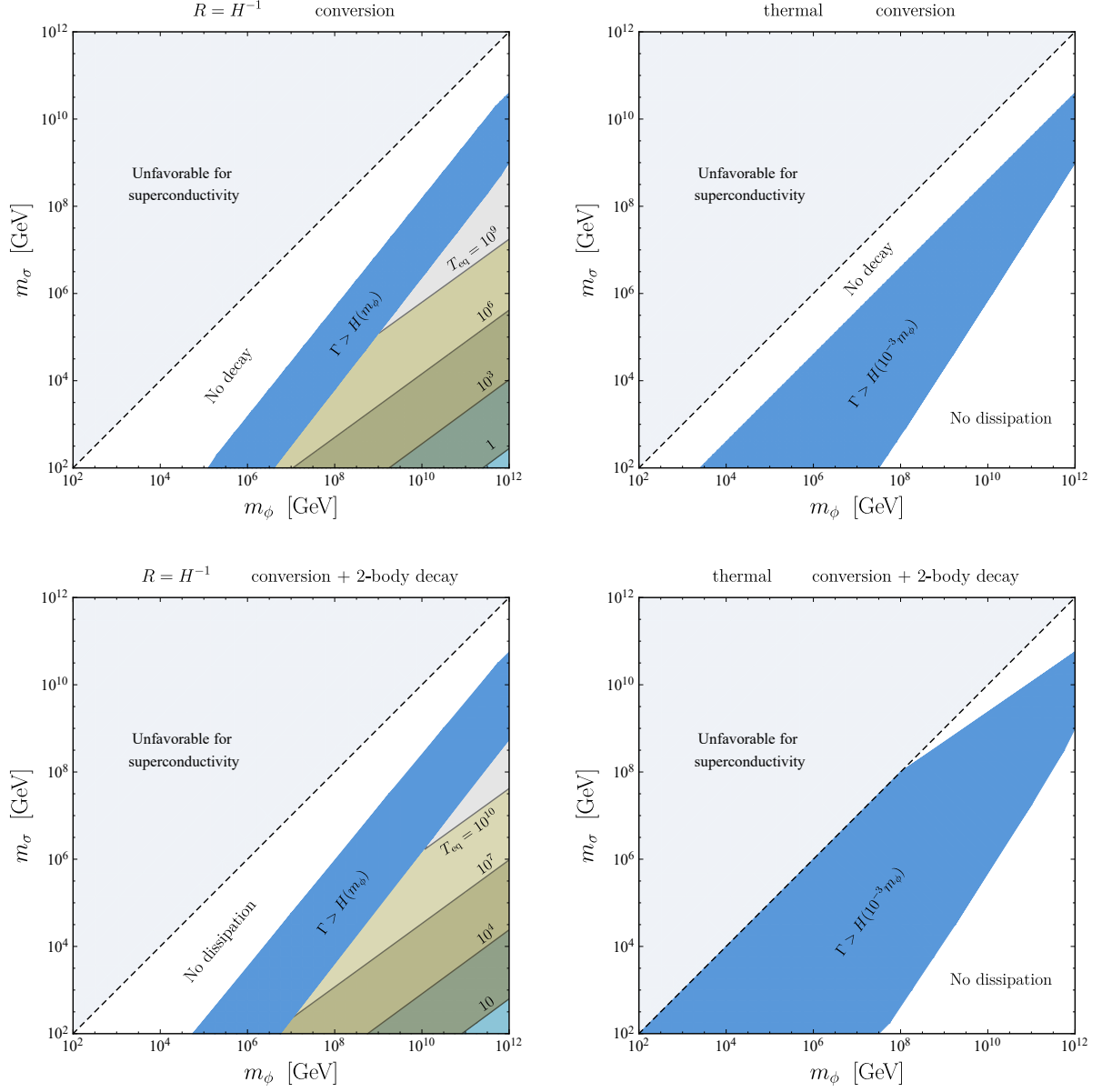


Figure 8: The parameter space where the decay of the zero mode with $E = m_\phi$ is significant, i.e., $\Gamma(T) > H(T)$ holds at some stage. These figures differ with respect to the type of string curves and decay processes as indicated. The contours correspond to the GeV-unit values of the temperature T_{eq} at which the transition from $\Gamma < H$ to $\Gamma > H$ occurs. The blue regions means $\Gamma > H$ is already met at the stage of the production of string network. The white blank regions represent the parameter space in which the zero mode survives at all stages, i.e., $\Gamma < H$ for arbitrary temperature.

but $\Gamma(T) < H(T)$ holds at any stage, resulting in no significant dissipation. Since the ratio $\Gamma(T)/H(T)$ for the thermal curve is UV-dominated, whether or not the decay is significant is determined at the highest temperature $T = 10^{-3}m_\phi$. That is why other color than blue regions cannot be seen in the right panels.

From the above results, we obtain the cosmological consequences of the zero mode decay. If the Yukawa coupling λ is tiny or absent, the two-body decay does not occur and the bottom panels in Fig. 8 are irrelevant. In this case, by taking into account both types of curves, superconducting strings cannot carry significant amount of current due to the rapid decay for $m_\phi \gg m_\sigma$ (typically, $m_\phi \gtrsim 10^2 m_\sigma$). This can be intuitively understood since the zero mode energy $E = m_\phi$ suffices to produce the on-shell bulk modes with the mass m_σ and to escape from the string. On the other hand, if a sizable Yukawa coupling λ is present, one should take into account also the bottom panels in Fig. 8. In this case, superconducting strings cannot carry significant current in almost all parameter region because, even with $m_\phi \approx m_\sigma$, the two-body decay is kinematically allowed and the thermal curve with $T = 10^{-3}m_\sigma$ is sufficient to cause a rapid decay. Note that there is an exceptional region $m_\sigma \approx m_\phi \gtrsim 10^8$ GeV (upper-right blank region in the bottom-right panel). The reason why the decay is suppressed for this region is that Γ/H at $T = 10^{-3}m_\phi$ is proportional to M_P/m_ϕ (see Eq. (4.14)).

4.3 Vorton stability

Throughout this paper, we only consider vortons that are sequentially produced from the string network [11, 34, 35]. Note that there are also vortons produced at the phase transition of the string formation. The latter ones typically have shorter lifetime due to less numbers of charges than the former, and thus the discussion on the former type is sufficient to study the stability of vortons.

In the VOS model, closed loops of strings are generated with the length $\sim 1/H(T_{\text{gen}})$ at $T = T_{\text{gen}}$. On these loops, the charge and current are randomly induced with the coherent length $1/T_{\text{gen}}$ thermally. It is expected [29] that the zero mode on closed loops becomes chiral (see Eq. (2.18)) as the loops contract. In the rest of the paper, we focus on such chiral vortons. Using the central limit theorem, we estimate the net charge value on the loop at the production, given as

$$Q(T_{\text{gen}}) \sim \sqrt{\frac{T_{\text{gen}}}{H(T_{\text{gen}})}} = \left(\frac{90}{\pi^2 g_*}\right)^{1/4} \sqrt{\frac{M_P}{T_{\text{gen}}}}. \quad (4.15)$$

At the classical level, after the production, the loop shrinks until the radius is stabilized, i.e., its size becomes $R_0 \sim Q/m_\phi$ (see Eq. (2.20)). Since the energy of the zero mode is given by $E \sim Q/R_0 \sim m_\phi$, we consider the zero mode decay width for $E = m_\phi$.

Similarly to the case of the string network, the zero mode decay in the vorton is caused by two types of string curves. One comes from the fact that a vorton is curved, i.e., its

radius of curvature is nothing but the radius of the stabilized loop R_0 . For this case, we again take L such that $\varepsilon = 1$ to avoid breakdown of the perturbativity. The other is the thermal curve from the interaction with thermal plasma. We consider the decay width for each type.

For the former type curve with a vorton produced at $T = T_{\text{gen}}$, the vorton radius depends on T_{gen} and so does the decay width Γ as

$$\Gamma_{\text{conv}}^{\text{vort}} \approx \Gamma_{\text{2-body}}^{\text{vort}} \approx \frac{m_\sigma^2 T_{\text{gen}}^{1/4}}{m_\phi M_P^{1/4}} \left[\log \left(\frac{m_\sigma}{m_\phi} \right) \right]^2 \quad \text{for } T_{\text{gen}} \gtrsim T_{\text{trs}}^{\text{vort}}, \quad (4.16)$$

and

$$\Gamma_{\text{conv}}^{\text{vort}} = 0, \quad \Gamma_{\text{2-body}}^{\text{vort}} \approx \lambda^2 \frac{m_\phi^3 T_{\text{gen}}^{3/4}}{m_\sigma^2 M_P^{3/4}} \left[\log \left(\frac{m_\sigma}{m_\phi} \right) \right]^2 \quad \text{for } T_{\text{gen}} \lesssim T_{\text{trs}}^{\text{vort}}, \quad (4.17)$$

where $T_{\text{trs}}^{\text{vort}} = M_P m_\sigma^2 / m_\phi^2$. We have used the series expansions for the Bessel functions $J_1(x) \sim x$ and $K_0(x) \sim (\log x)^2$, and dropped $\mathcal{O}(1)$ numerical coefficients. (The above expressions are numerically confirmed in Appendix C.) As mentioned in the last subsection, the two partial decay widths Γ_{conv} and $\Gamma_{\text{2-body}}$ agree in the high temperature region $T_{\text{gen}} \gtrsim T_{\text{trs}}^{\text{vort}}$, while the conversion process is kinematically forbidden in the low temperature region.

For the latter type curve with thermal plasma, the decay width does not depend on T_{gen} but on T . (T_{gen} labels each vorton as its production time while T is used as the temporal variable.) The partial widths are the same as those in the last subsection (Eqs. (4.13) and (4.14) for their approximate expressions).

After the zero mode decay occurs with the time scale $1/\Gamma$, its charge decreases by a unit charge, which results in that the vorton shrinks and becomes balanced at a radius $R \sim (Q - 1)/m_\phi$. Then the zero mode can decay again with the time scale $1/\Gamma$ in which the classically stable radius R_0 is replaced by $\sim (Q - 1)/m_\phi$. Thus the time evolution of the radius R of a vorton produced at $T = T_{\text{gen}}$ is described by the following equation:

$$\frac{\dot{R}}{R} = \frac{\dot{Q}}{Q} = -\Gamma(R, T), \quad (4.18)$$

with the initial condition

$$R|_{T=T_{\text{gen}}} = R_0(T_{\text{gen}}) \sim \frac{Q(T_{\text{gen}})}{m_\phi}. \quad (4.19)$$

(The dotted quantities indicate their derivatives with respect to the cosmic time t .) After shrinking sufficiently with Eq. (4.18), the vorton eventually becomes to have a radius comparable to the string width $1/m_\phi$, which is regarded as the death of the vorton.

Fig 9 shows the time-evolution of the vorton radius with $m_\phi = 10^{12}$ GeV and $m_\sigma = 10^2$ GeV. The black lines with arrows indicate the trajectories of the vorton radii with

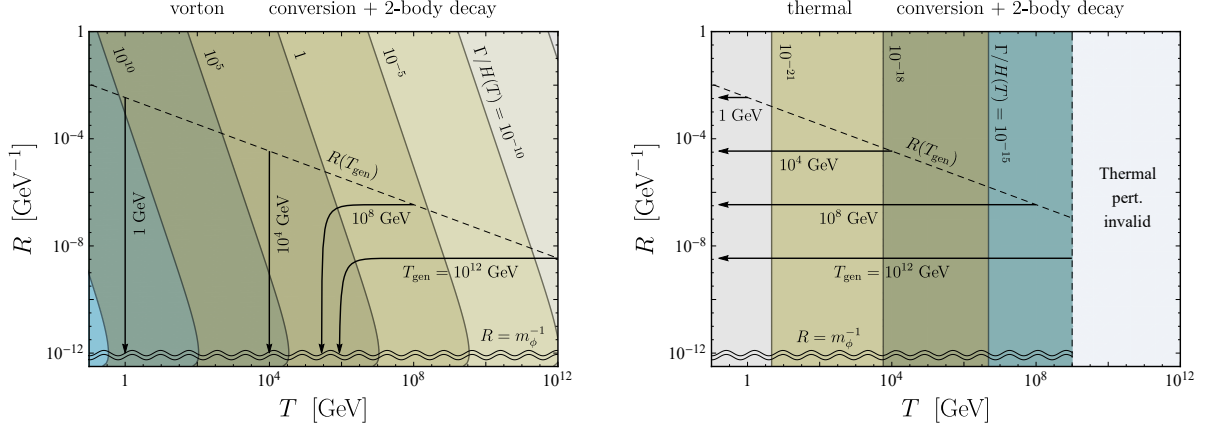


Figure 9: The time evolution of the vorton radius R with various production temperatures in the cases of the vorton curve (left) and the thermal curve (right). The model parameters are set to be $E = m_\phi = 10^{12}$ GeV and $m_\sigma = 10^2$ GeV. The black lines with arrows indicate the trajectories of vorton radii produced at $T = T_{\text{gen}}$. Each contour means the specified values of decay widths over the Hubble parameter.

various T_{gen} . The decay widths include both the processes of the conversion and the two-body decay (with $\lambda = 1$). In the left panel, we consider the decay due to the vorton curve, while the thermal one is considered in the right panel. Each contour means the value of Γ/H . We can find that once Γ exceeds H , the vorton radius immediately shrinks into $R = m_\phi^{-1}$, the death of the vorton, which means that vortons die approximately when $\Gamma = H$. The contribution from the thermal curves is not dominant to the decay for these mass parameters because the string is too heavy to be deformed by thermal plasma.

Fig. 10 shows the time evolution of the vorton radius for various values of m_σ with m_ϕ fixed to be 10^{12} GeV. The solid, dashed and dotted lines with arrows indicate the trajectories of the vorton radii for various m_σ and T_{gen} . The top (bottom) two panels correspond to the conversion process (the conversion and the two-body decay with $\lambda = 1$). The left panels correspond to the vorton curve while the right panels to the thermal one. In the gray region with “Thermal pert. invalid”, the temperature T does not satisfy the condition Eq. (4.10) and hence the calculation is not reliable. Thus the vortons in such regions are assumed to be stable against the thermal curves. We find that particularly the two-body decay due to the vorton curves (bottom-left panel) is significant than the others. The thermal ones do not cause the strong decay since the thermal curves become effective at higher temperature.

Fig. 11 shows the parameter space (m_σ, m_ϕ) by colored regions in which some of the vortons die by now due to the decay of the current and charge. The black contours in the colored regions indicate the values of $T_{\text{gen}}^{\text{max}}$, defined as the maximum T_{gen} among the living vortons in the present Universe, i.e., the temperature at which the oldest living

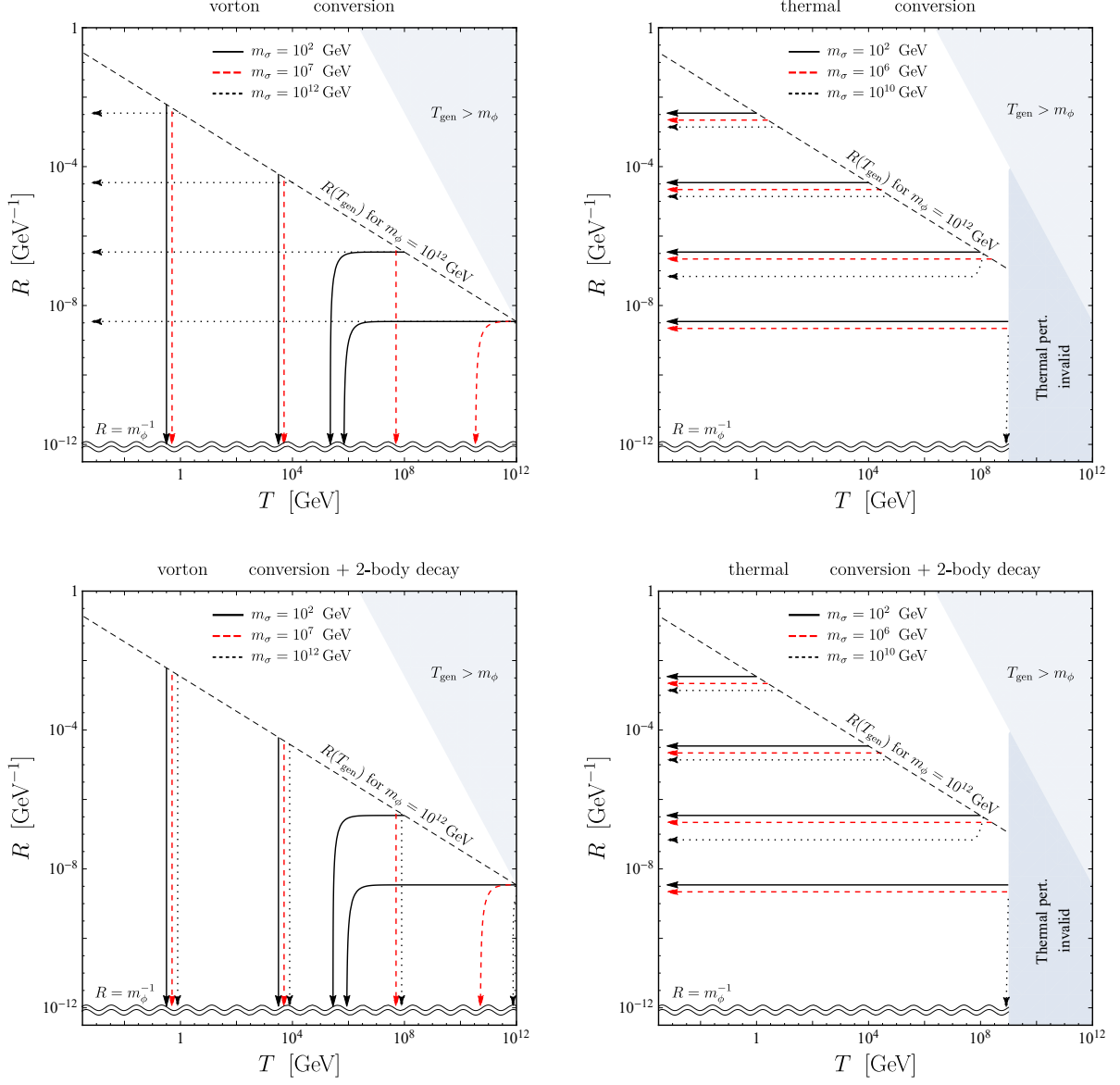


Figure 10: The time evolution of the vorton radius R with various production temperatures and $E = m_\phi = 10^{12}$ GeV. The lines with arrows indicates the trajectories of the vorton radii for different m_σ and T_{gen} . These figures differ with respect to the type of string curves and decay processes as indicated. In the gray regions, the temperature T does not satisfy the condition Eq. (4.10) and we assume no decay process occurs in the regions.

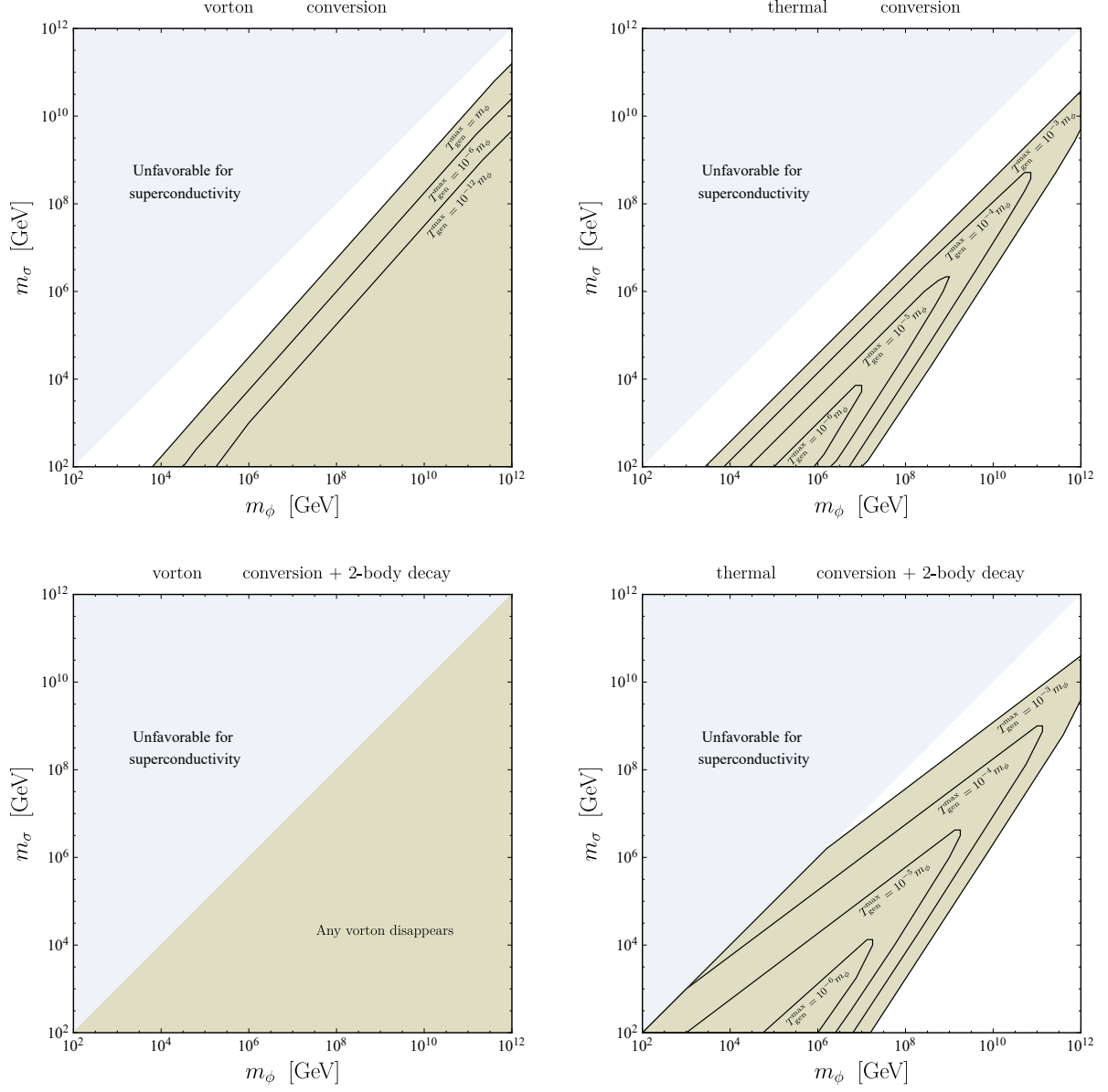


Figure 11: The parameter spaces for (m_σ, m_ϕ) where the vortons are dead by now. We set $E = m_\phi$. The black contours in the colored regions indicate the values of $T_{\text{gen}}^{\text{max}}$, defined as the maximum T_{gen} among the living vortons in the present Universe. In the white blank regions, all vortons survive in the present Universe. These figures differ with respect to the type of string curves and decay processes as indicated. The upper-left gray regions in the plots are unfavorable to the superconductivity.

vortons were produced. In the white blank regions, all vortons are stable and survive in the present Universe. The top (bottom) two panels correspond to the conversion process (the conversion and two-body decay processes). The left panels correspond to the vorton curves while the right panels to the thermal ones. The upper-left gray regions in the plots are unfavorable to the superconductivity. We can see that the vorton curve is more crucial for the vorton lifetime than the thermal one.

From these figures, we obtain the effects of zero mode decay on the vorton stability. Once one takes into account the two-body decay process with the (sizable) Yukawa coupling λ , the vortons cannot be stable due to the zero mode decay caused by the vorton curves (bottom-left panel). On the other hand, the vortons can be stable if the model does not contain such a decay process and the mass parameters m_σ and m_ϕ are not so hierarchical, $10^{-2} \lesssim m_\sigma/m_\phi \lesssim 1$, which forbids the decay kinematically, as seen in the white regions in the top two panels.

5 Conclusion

In this work, we studied the stability of zero modes traveling along the bosonic superconducting string. In particular, we focused on the zero mode quantum decay via the deformation of the straight string solution. This deformation is treated as string curves of several types and the effective interaction vertices including the string deformation are evaluated. Then we calculated the decay widths for the conversion to bulk massive modes and the two-body decay to bulk light fermions. The approximate forms of the decay widths were derived by regarding the scalar mass as a square well potential. We numerically evaluated the behavior of these decay widths and found the parameter space where stable superconducting current and vortons are able to exist. These results are summarized in Figs. 8 and 11.

In the present $U(1) \times \tilde{U}(1)$ model, the hierarchy among mass parameters is not favored if superconducting strings survive to the present Universe. The vortons could have somewhat long lifetime but the current on the vortons disappear due to the quantum decay processes at some stage. Even in this case, the vortons and their decays may have impacts on cosmology. We considered the behavior of superconducting current in the model where two complex scalars are introduced. This minimal setup has a few number of couplings and the existence of the superconducting solution requires constraints on the parameters. That leads to a similar magnitude between the widths of string and of the potential trapping the zero mode. In more general models admitting the bosonic superconductivity, these widths can be different and the parameter space for the existence of long-lived currents may be different from our results. For example, in the DFSZ model, two Higgs doublets and one Peccei-Quinn scalar are introduced, whose interactions are

suppressed by a large Peccei-Quinn scale. This model has a possibility that the conditions for the existence of stable superconducting strings and vortons are relaxed, and there can be more long-lived objects in wider parameter space. It is worth considering cosmological impacts of these charged objects in the DFSZ model. We leave it as future work.

Acknowledgments

The authors would like to thank Keisuke Harigaya, Koji Hashimoto, and Kai Schmitz for useful discussions and comments. This work is supported in part by JSPS KAKENHI Grant Numbers JP21J01117 (YH) and JP20K03949 (KY).

A Scalar Lagrangian

The scalar Lagrangian of the $U(1) \times \tilde{U}(1)$ model is originally given by (2.1) with the real couplings λ_ϕ , λ_σ , and κ . Around the classical string background ϕ_{cl} and σ_{cl} , the scalar fields are described by $\Phi = \phi_{\text{cl}} + \phi$ and $\Sigma = \sigma_{\text{cl}} + \sigma$. Substituting them into the Lagrangian and using the EOMs for ϕ_{cl} and σ_{cl} , we find the scalar Lagrangian for the quantum fields ϕ and σ :

$$\begin{aligned}
\mathcal{L} = & |\partial_\mu \phi|^2 + |\partial_\mu \sigma|^2 - \frac{\lambda_\phi}{4} |\phi|^4 - \frac{\lambda_\sigma}{4} |\sigma|^4 - \kappa |\phi|^2 |\sigma|^2 \\
& - \frac{\lambda_\phi}{4} \left[(\phi_{\text{cl}}^* \phi + \phi_{\text{cl}} \phi^*)^2 + 2(|\phi_{\text{cl}}|^2 - v_\phi^2) |\phi|^2 \right] \\
& - \frac{\lambda_\sigma}{4} \left[(\sigma_{\text{cl}}^* \sigma + \sigma_{\text{cl}} \sigma^*)^2 + 2(|\sigma_{\text{cl}}|^2 - v_\sigma^2) |\sigma|^2 \right] \\
& - \kappa \left[(\phi_{\text{cl}}^* \phi + \phi_{\text{cl}} \phi^*) (\sigma_{\text{cl}}^* \sigma + \sigma_{\text{cl}} \sigma^*) + |\sigma_{\text{cl}}|^2 |\phi|^2 + |\phi_{\text{cl}}|^2 |\sigma|^2 \right] \\
& - \frac{\lambda_\phi}{2} (\phi_{\text{cl}}^* \phi + \phi_{\text{cl}} \phi^*) |\phi|^2 - \frac{\lambda_\sigma}{2} (\sigma_{\text{cl}}^* \sigma + \sigma_{\text{cl}} \sigma^*) |\sigma|^2 \\
& - \kappa \left[(\sigma_{\text{cl}}^* \sigma + \sigma_{\text{cl}} \sigma^*) |\phi|^2 + (\phi_{\text{cl}}^* \phi + \phi_{\text{cl}} \phi^*) |\sigma|^2 \right] \\
& + \frac{\lambda_\phi}{4} (|\phi_{\text{cl}}|^4 - v_\phi^4) + \frac{\lambda_\sigma}{4} (|\sigma_{\text{cl}}|^4 - v_\sigma^4) - \kappa |\phi_{\text{cl}}|^2 |\sigma_{\text{cl}}|^2. \tag{A.1}
\end{aligned}$$

The first line includes the kinetic terms and the genuine interactions of the quantum fields. The following three lines are quadratic in the quantum fields, that is, the mass terms in the string background. The next two line contains the scalar cubic interactions, and the last one just the constant.

When we decompose ϕ and σ as

$$\phi = \frac{\phi_R + i\phi_I}{\sqrt{2}}, \quad \sigma = \frac{\sigma_R + i\sigma_I}{\sqrt{2}}, \tag{A.2}$$

and assume σ_{cl} is real-valued, the scalar mass matrix in the string background reads

$$\mathcal{M} = \begin{pmatrix} \frac{\lambda_\phi}{2}(|\phi_{\text{cl}}|^2 - v_\phi^2) & \lambda_\phi(\text{Re } \phi_{\text{cl}})(\text{Im } \phi_{\text{cl}}) & 2\kappa(\text{Re } \phi_{\text{cl}})\sigma_{\text{cl}} & \\ +\kappa\sigma_{\text{cl}}^2 + \lambda_\phi(\text{Re } \phi_{\text{cl}})^2 & & & \\ \lambda_\phi(\text{Re } \phi_{\text{cl}})(\text{Im } \phi_{\text{cl}}) & \frac{\lambda_\phi}{2}(|\phi_{\text{cl}}|^2 - v_\phi^2) & 2\kappa(\text{Im } \phi_{\text{cl}})\sigma_{\text{cl}} & \\ +\kappa\sigma_{\text{cl}}^2 + \lambda_\phi(\text{Im } \phi_{\text{cl}})^2 & & & \\ 2\kappa(\text{Re } \phi_{\text{cl}})\sigma_{\text{cl}} & 2\kappa(\text{Im } \phi_{\text{cl}})\sigma_{\text{cl}} & \frac{\lambda_\sigma}{2}(3\sigma_{\text{cl}}^2 - v_\sigma^2) & \\ & & + \kappa|\phi_{\text{cl}}|^2 & \\ & & & \frac{\lambda_\sigma}{2}(\sigma_{\text{cl}}^2 - v_\sigma^2) & \\ & & & + \kappa|\phi_{\text{cl}}|^2 \end{pmatrix} \quad (\text{A.3})$$

in the $(\phi_R, \phi_I, \sigma_R, \sigma_I)$ basis. One can see that σ_I , which contains the zero mode (the current carrier of superconductivity), is decoupled from the other scalars in the quadratic order. The other three modes mix with each other via the position-dependent quadratic couplings. Its diagonalization is not necessarily useful since it generally turns out to induce complex kinetic terms. We also notice that the Lagrangian has a Z_2 parity under which σ_I is odd. It is originated from the CP symmetry in the Σ sector, $\Sigma \leftrightarrow \Sigma^*$. That restricts the interaction form, in particular, there is no decay vertex of σ_I (no term involving the first power of σ_I).

In the case of straight string, the position-dependent mass of σ_I is defined by

$$M_I^2(r) = \frac{\lambda_\sigma}{2}(\hat{\sigma}^2 - v_\sigma^2) + \kappa|\hat{\phi}|^2. \quad (\text{A.4})$$

The string profile functions have the asymptotic behavior $f(r) \rightarrow 1$ and $h(r) \rightarrow 0$ far from the string, and then we find $M_I^2(r) \rightarrow m_\sigma^2$. In the same limit, σ_R also has a mass m_σ . On the other hand, the ϕ sector contains two mass eigenvalues 0 and $m_\phi^2 = \lambda_\phi v_\phi^2$. The massless mode is the direction $(\text{Re } \hat{\phi})\phi_I - (\text{Im } \hat{\phi})\phi_R$, the Nambu-Goldstone boson associated with the $\tilde{U}(1)$ breaking.

B Propagator in the string background

We present the formal expression of the four-dimensional propagator for the $\sigma_I(x)$ field that is defined by

$$\langle 0 | T \sigma_I(x) \sigma_I(x') | 0 \rangle = G(x, x'). \quad (\text{B.1})$$

The propagator $G(x, x')$ is the inverse of the Klein-Gordon operator in the string background

$$[\square + M_I^2(r)]G(x, x') = \delta^4(x - x'), \quad (\text{B.2})$$

where the position-dependent mass operator M_I^2 is defined by (3.10). Performing the Fourier transformation with respect to the t, z, θ variables, we have

$$\left[\frac{-1}{r} \partial_r (r \partial_r) + \frac{l^2}{r^2} + M_I^2(r) - \mathbf{k}^2 \right] G_{\mathbf{k}}^l(r, r') = \frac{1}{r} \delta(r - r'), \quad (\text{B.3})$$

$$G(x, x') = \int \frac{d^2 \mathbf{k}}{(2\pi)^3} \sum_l G_{\mathbf{k}}^l(r, r') e^{-i\mathbf{k} \cdot (\mathbf{x} - \mathbf{x}')} e^{il(\theta - \theta')}. \quad (\text{B.4})$$

First, dropping the right-handed side of (B.3), we solve the equation in the region $r \in [r_0, r_\infty]$ (e.g., r_0 and r_∞ mean the UV and infrared (IR) cutoff, respectively). Before specifying the boundary conditions at $r = r_0$ and $r = r_\infty$, we have two independent solutions $\varphi_1(r)$ and $\varphi_2(r)$. These solutions depend on the momenta \mathbf{k} and l . Here and hereafter we do not explicitly show these momentum indices for notation simplicity. With these solution at hand, the propagator is written down as

$$G_{<}(r, r') = A_{<}(r') \varphi_1(r) + B_{<}(r') \varphi_2(r) \quad \text{for } r < r', \quad (\text{B.5})$$

$$G_{>}(r, r') = A_{>}(r') \varphi_1(r) + B_{>}(r') \varphi_2(r) \quad \text{for } r > r'. \quad (\text{B.6})$$

The constants of integration $A_{<}, A_{>}, B_{<}, B_{>}$ are determined by the boundary conditions and matching in the following way.

Let us consider the Neumann conditions at both boundaries. That implies

$$A_{<}(r') \varphi_1'(r_0) + B_{<}(r') \varphi_2'(r_0) = 0, \quad (\text{B.7})$$

$$A_{>}(r') \varphi_1'(r_\infty) + B_{>}(r') \varphi_2'(r_\infty) = 0, \quad (\text{B.8})$$

where φ_i' denotes the derivative of φ_i . The propagators in the two regions ($r < r'$ and $r > r'$) are matched at $r = r'$ taking into account the right-handed side of (B.3). The continuity of wavefunctions and the discontinuity of the slopes which follows from the integration of (B.3) around $r = r'$ lead to the matching conditions

$$A_{<}(r') \varphi_1(r') + B_{<}(r') \varphi_2(r') = A_{>}(r') \varphi_1(r') + B_{>}(r') \varphi_2(r'), \quad (\text{B.9})$$

$$A_{<}(r') \varphi_1'(r') + B_{<}(r') \varphi_2'(r') = A_{>}(r') \varphi_1'(r') + B_{>}(r') \varphi_2'(r') + \frac{1}{r'}. \quad (\text{B.10})$$

With all these conditions, we can fix the constants of integration and find the propagator

$$G_{\mathbf{k}}^{l(\text{NN})}(r, r') = \frac{g_p(r_>, r_0) g_p(r_>, r_\infty)}{r' g_p(r', r') g_{pp}(r_\infty, r_0)}, \quad (\text{B.11})$$

where $r_{<} (r_{>})$ stands for the lesser (greater) of r and r' . The index NN is attached to indicate that the propagator satisfies the Neumann boundary conditions at $r = r_0$ and $r = r_\infty$. The functions g_p and g_{pp} are defined as

$$g(r_1, r_2) = \varphi_1(r_1) \varphi_2(r_2) - \varphi_1(r_2) \varphi_2(r_1), \quad (\text{B.12})$$

$$g_p(r_1, r_2) = \partial_{r_2} g(r_1, r_2), \quad (\text{B.13})$$

$$g_{pp}(r_1, r_2) = \partial_{r_1} \partial_{r_2} g(r_1, r_2). \quad (\text{B.14})$$

It is easy to verify that $G_k^{l(\text{NN})}$ satisfies $[\frac{-1}{r} \partial_r (r \partial_r) + l^2/r^2 + M_I^2(r) - k^2] G_k^{l(\text{NN})}(r, r') = [\frac{-1}{r'} \partial_{r'} (r' \partial_{r'}) + l^2/r'^2 + M_I^2(r') - k^2] G_k^{l(\text{NN})}(r, r') = 0$ at $r \neq r'$, noting that $[\frac{-1}{r} \partial_r (r \partial_r) + l^2/r^2 + M_I^2(r) - k^2] g_p(r, r') = [\frac{-1}{r} \partial_r (r \partial_r) + l^2/r^2 + M_I^2(r) - k^2] (r g_p(r, r')) = 0$.

The propagators for the other boundary conditions can be found in parallel ways as

$$G_k^{l(\text{ND})}(r, r') = \frac{g_p(r_<, r_0) g(r_>, r_\infty)}{r' g_p(r', r') g_p(r_\infty, r_0)}, \quad (\text{B.15})$$

$$G_k^{l(\text{DN})}(r, r') = \frac{g(r_0, r_<) g_p(r_>, r_\infty)}{r' g_p(r', r') g_p(r_0, r_\infty)}, \quad (\text{B.16})$$

$$G_k^{l(\text{DD})}(r, r') = \frac{g(r_0, r_<) g(r_>, r_\infty)}{r' g_p(r', r') g(r_0, r_\infty)}, \quad (\text{B.17})$$

where the superscript D denotes the Dirichlet boundary condition, for example, $G^{(\text{DD})}$ vanishes at both boundaries.

The mass spectrum in the effective theory is extracted from the poles of propagators. From (B.11), we find the pole condition

$$0 = g_{pp}(r_\infty, r_0) = \varphi_1'(r_\infty) \varphi_2'(r_0) - \varphi_1'(r_0) \varphi_2'(r_\infty). \quad (\text{for NN}) \quad (\text{B.18})$$

Remembering $\varphi_{1,2}$ depend on the momenta k and l , this equation determines k^2 in terms of l , $r_{0,\infty}$, and other quantities. For the other-type of propagators, we have

$$0 = g_p(r_\infty, r_0) = \varphi_1(r_\infty) \varphi_2'(r_0) - \varphi_1'(r_0) \varphi_2(r_\infty), \quad (\text{for ND}) \quad (\text{B.19})$$

$$0 = g_p(r_0, r_\infty) = \varphi_1(r_0) \varphi_2'(r_\infty) - \varphi_1'(r_\infty) \varphi_2(r_0), \quad (\text{for DN}) \quad (\text{B.20})$$

$$0 = g(r_0, r_\infty) = \varphi_1(r_0) \varphi_2(r_\infty) - \varphi_1(r_\infty) \varphi_2(r_0). \quad (\text{for DD}) \quad (\text{B.21})$$

The zero mode ($k^2 = l = 0$) is expected to be found in the spectrum (B.19) (see the boundary condition for the string profile functions (2.8)).

As an application, we consider the propagator for an approximate mass operator (3.31). We first solve (B.3) setting the right-handed side to zero. Two independent solutions are obtained by taking account of the continuities of wavefunctions and their slopes at $r = r_b$. The explicit forms of the solutions are

$$\varphi_1(r) = \begin{cases} J_l(\bar{M}r) + u(\bar{m}_\sigma, \bar{M}) H_l(\bar{M}r) & \text{for } r < r_b, \\ v(\bar{m}_\sigma, \bar{M}) H_l(\bar{m}_\sigma r) & \text{for } r > r_b, \end{cases} \quad (\text{B.22})$$

$$\varphi_2(r) = \begin{cases} v(\bar{M}, \bar{m}_\sigma) H_l(\bar{M}r) & \text{for } r < r_b, \\ J_l(\bar{m}_\sigma r) + u(\bar{M}, \bar{m}_\sigma) H_l(\bar{m}_\sigma r) & \text{for } r > r_b. \end{cases} \quad (\text{B.23})$$

where $\bar{M}^2 = M^2 + \mathbf{k}^2$, $\bar{m}_\sigma^2 = -m_\sigma^2 + \mathbf{k}^2$, and J_l (H_l) are the Bessel (Hankel) functions of the first kind. The functions u and v are defined by

$$u(\alpha, \beta) = \frac{J_l(\beta r_b) \alpha H'_l(\alpha r_b) - \beta J'_l(\beta r_b) H_l(\alpha r_b)}{H_l(\alpha r_b) \beta H'_l(\beta r_b) - \alpha H'_l(\alpha r_b) H_l(\beta r_b)}, \quad (\text{B.24})$$

$$v(\alpha, \beta) = \frac{2i/\pi r_b}{H_l(\alpha r_b) \beta H'_l(\beta r_b) - \alpha H'_l(\alpha r_b) H_l(\beta r_b)}. \quad (\text{B.25})$$

The propagator, e.g., $G_k^{l(\text{NN})}$ for the Neumann boundary conditions at both sides, is obtained from (B.11) with these solutions $\varphi_{1,2}$. The dominant contribution to the zero mode decay may be given by the mediator with the Neumann conditions at both boundaries, which means that it interacts with the zero mode in the string and can also escape to the outside of the string. Such process is described by the propagator between the UV and IR cutoff scales, which is found to take an approximate value $G_k^{l(\text{NN})}(r_0, r_\infty) \sim (\bar{m} \bar{M} r_b r_0)^l / (\bar{m} r_\infty)^{1/2}$.

C Temperature dependence of Γ

We here present the numerical plots for the temperature T dependence of the zero mode decay width Γ for two types of string curves: the curve with $R = H^{-1}$ in the string network (Fig. 12) and the thermal one (Fig. 13). Both the figures show the values of Γ in the (m_ϕ, T) -plane with fixed m_σ and the (m_σ, T) -plane with fixed m_ϕ . The top (bottom) two panels correspond to the conversion process (the conversion and two-body decay processes). The shaded regions represent that the zero mode current cannot be significant, $\Gamma(T) > H(T)$, at the temperature T . The values around the contours are given in GeV unit. The gray regions with “ $T > m_\phi$ ” and “Thermal pert. invalid” are excluded for the reasons that the string network does not exist and that the condition $T < 10^{-3} m_\phi$ is not satisfied, respectively. These plots agree well with the asymptotic expressions given in Eqs. (4.11)–(4.14).

On the other hand, the decay width Γ due to the vorton curve does not depend on T but on T_{gen} , as mentioned in Sec. 4. Fig. 14 shows T_{gen} -dependence of Γ for each vorton generated at $T = T_{\text{gen}}$ in the (m_ϕ, T_{gen}) and $(m_\sigma, T_{\text{gen}})$ planes in the top and bottom panels, respectively. The left (right) panels are calculated by considering the conversion (the conversion and the two-body decay). The contours correspond to the values of Γ in GeV unit. The shaded regions indicate that the decay is significant compared to the Hubble parameter, $\Gamma(T_{\text{gen}}) > H(T_{\text{gen}})$. In the white “No decay” region, the condition (3.23) is not satisfied, forbidding the conversion kinematically. The upper-left gray regions in the top panels are excluded since the string network does not exist when $T > m_\phi$. These plots agree with the asymptotic expressions in Eqs. (4.16) and (4.17).

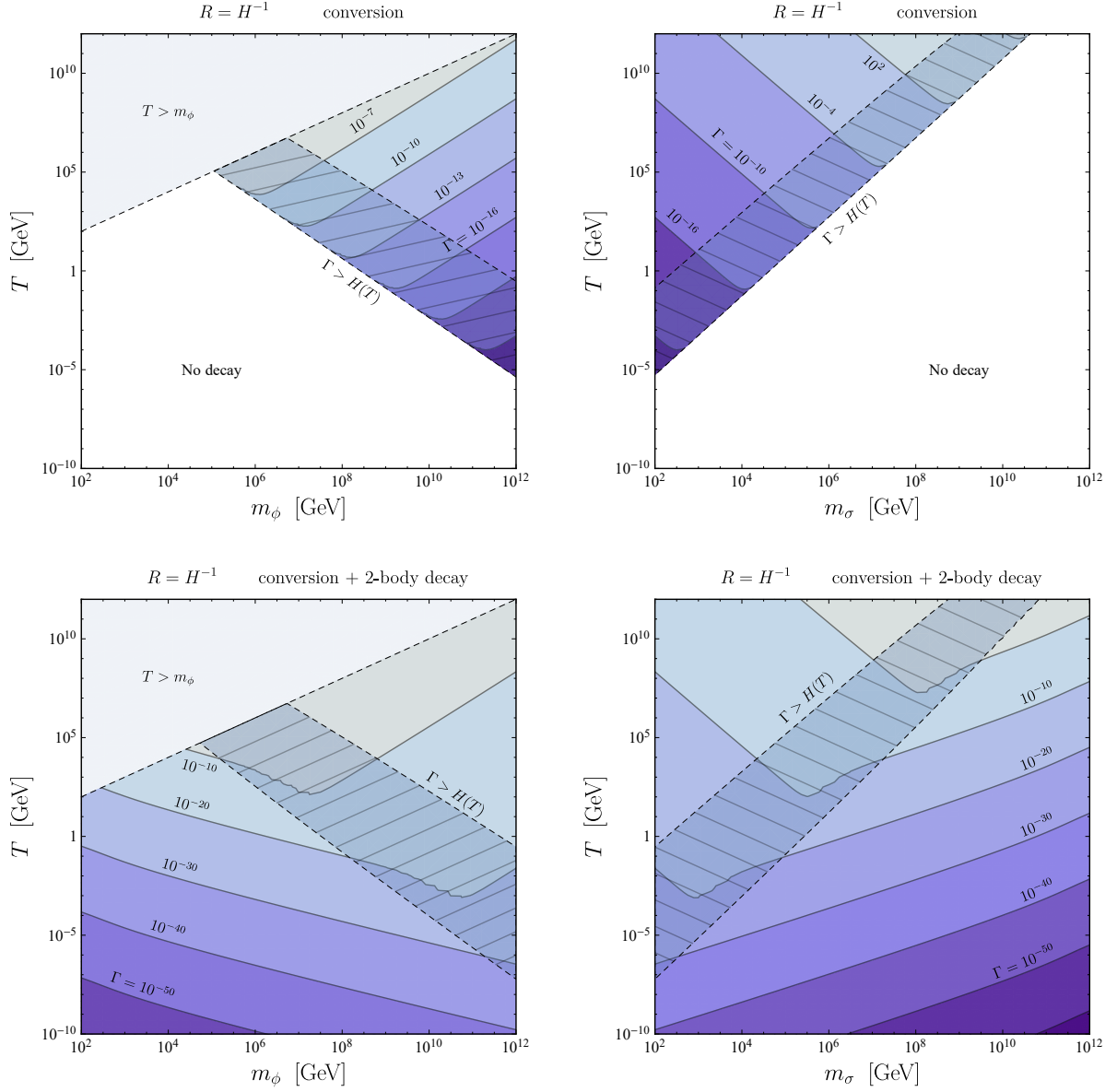


Figure 12: The decay width caused by the string curve with $R = H^{-1}$ in the (m_ϕ, T) -plane ($m_\sigma = 10^2$ GeV) and in the (m_σ, T) -plane ($m_\phi = 10^{12}$ GeV). The top (bottom) two panels correspond to the conversion process (the conversion and two-body decay processes). The values around the contours are given in GeV unit. In the white blank regions, the conversion process is kinematically forbidden. The gray regions with “ $T > m_\phi$ ” is excluded since the string network does not exist.

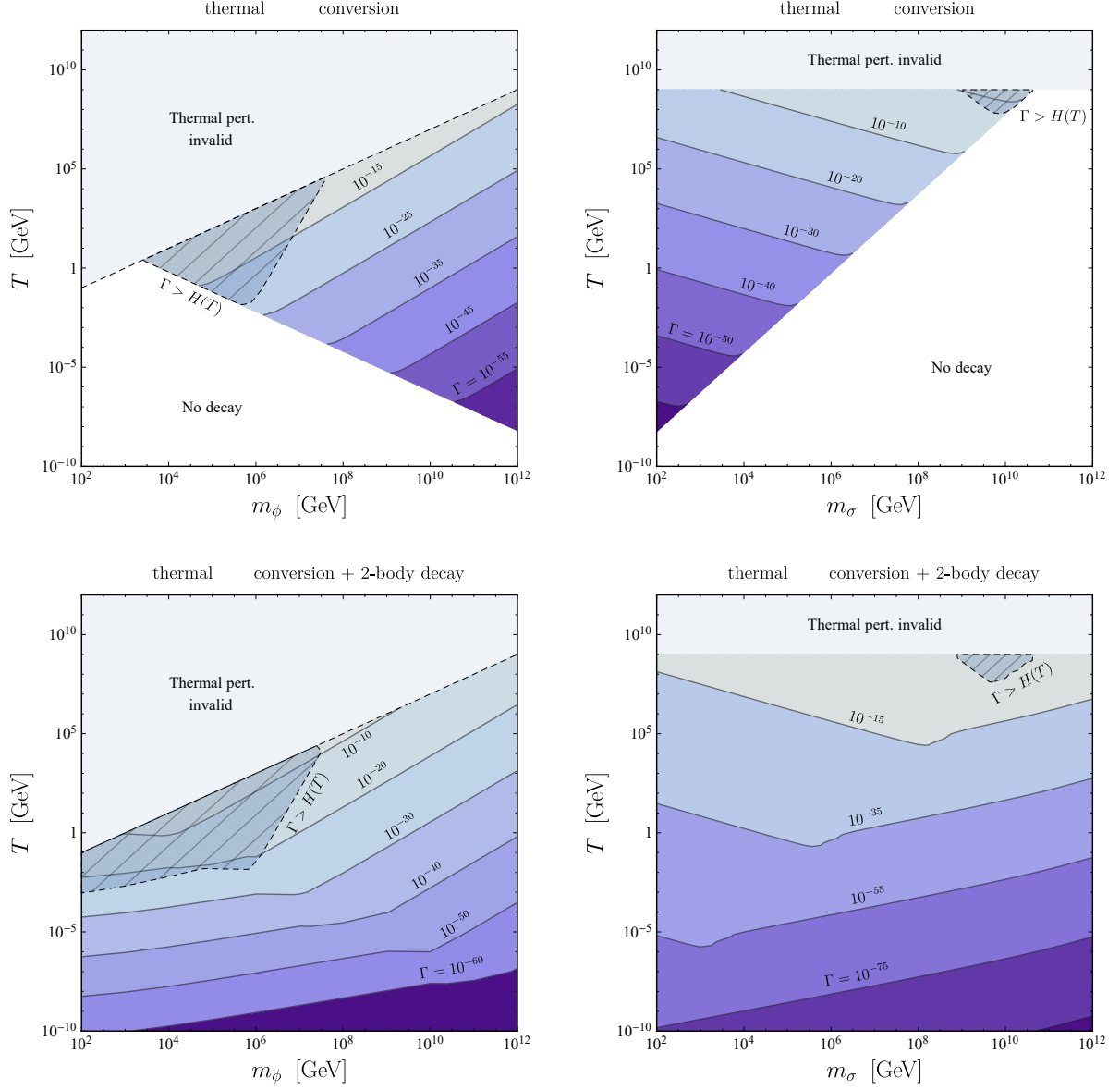


Figure 13: The decay width caused by the thermal curve in the (m_ϕ, T) -plane ($m_\sigma = 10^2$ GeV) and in the (m_σ, T) -plane ($m_\phi = 10^{12}$ GeV). The top (bottom) two panels correspond to the conversion process (the conversion and two-body decay processes). The values around the contours are given in GeV unit. In the white blank regions, the conversion process is kinematically forbidden. The gray regions with “Thermal pert. invalid” is excluded since the condition $T < 10^{-3}m_\phi$ is not satisfied.

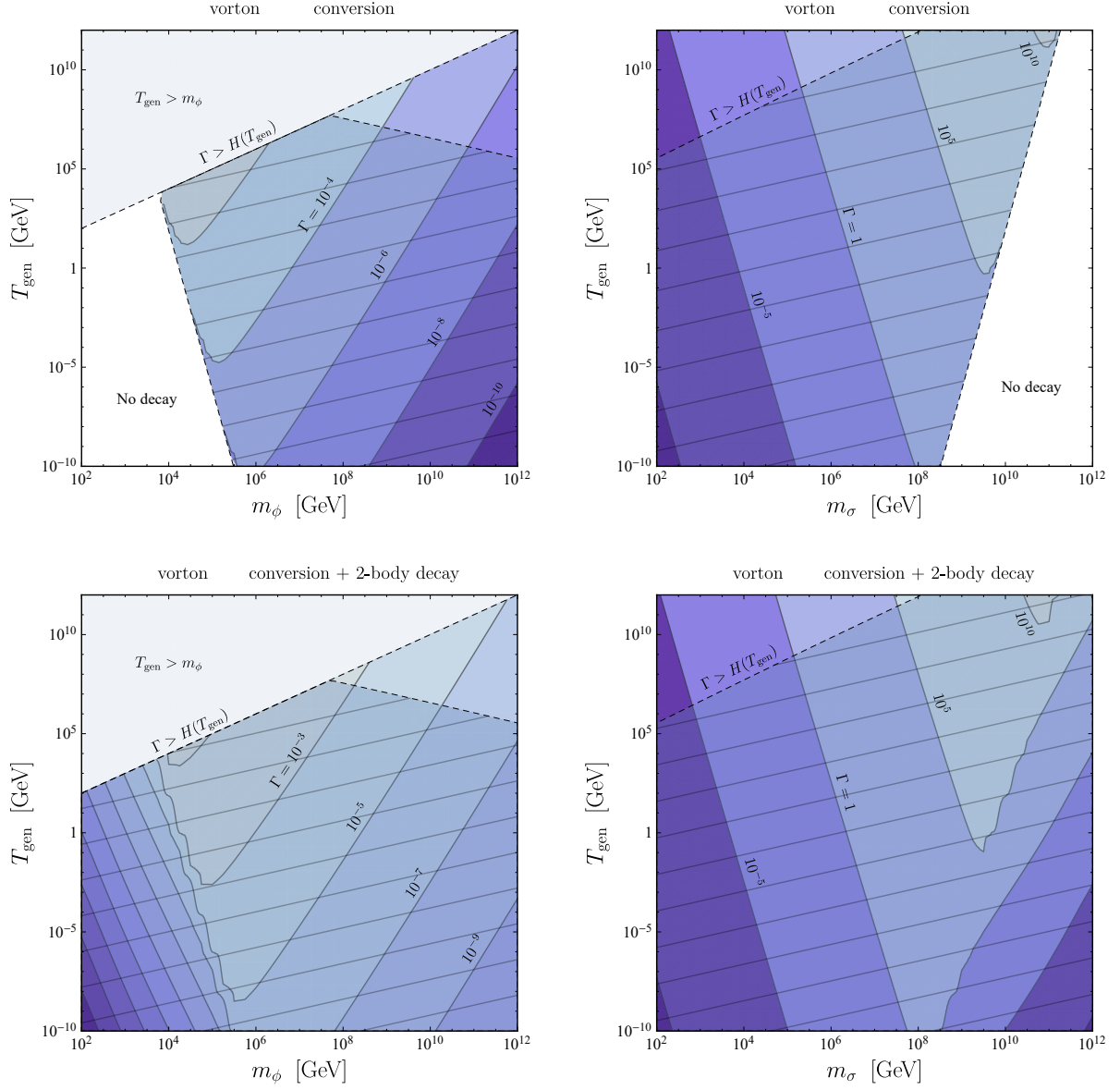


Figure 14: The values of Γ in GeV unit for classically stable vortons produced at the temperature $T = T_{\text{gen}}$ are shown in the (m_ϕ, T_{gen}) -plane ($m_\sigma = 10^2$ GeV) and in the $(m_\sigma, T_{\text{gen}})$ -plane ($m_\phi = 10^{12}$ GeV). The decay is assumed to be caused by the vorton curvature via the conversion (top panels) and the conversion and two-body decay (bottom panels). The white regions with “No decay” corresponds to the region in which the conversion process is kinematically forbidden.

References

- [1] A. Vilenkin and E. P. S. Shellard, *Cosmic Strings and Other Topological Defects*. Cambridge University Press, 7, 2000.
- [2] R. Caldwell *et al.*, *Detection of Early-Universe Gravitational Wave Signatures and Fundamental Physics*, [arXiv:2203.07972 \[gr-qc\]](#).
- [3] **LISA Cosmology Working Group** Collaboration, P. Auclair *et al.*, *Cosmology with the Laser Interferometer Space Antenna*, [arXiv:2204.05434 \[astro-ph.CO\]](#).
- [4] R. Jackiw and P. Rossi, *Zero Modes of the Vortex - Fermion System*, *Nucl. Phys. B* **190** (1981) 681–691.
- [5] E. Witten, *Superconducting Strings*, *Nucl. Phys. B* **249** (1985) 557–592.
- [6] J. P. Ostriker, A. C. Thompson, and E. Witten, *Cosmological Effects of Superconducting Strings*, *Phys. Lett. B* **180** (1986) 231–239.
- [7] R. Jeannerot, *A New mechanism for leptogenesis*, *Phys. Rev. Lett.* **77** (1996) 3292–3295 [[arXiv:hep-ph/9609442](#)].
- [8] G. Lazarides and Q. Shafi, *Superconducting Strings in Axion Models*, *Phys. Lett. B* **151** (1985) 123–126.
- [9] N. Ganoulis and G. Lazarides, *Fermionic Zero Modes for Cosmic Strings*, *Nucl. Phys. B* **316** (1989) 443–455.
- [10] A. Iwazaki, *Spontaneous magnetization of axion domain wall and primordial magnetic field*, *Phys. Rev. Lett.* **79** (1997) 2927–2930 [[arXiv:hep-ph/9705456](#)].
- [11] H. Fukuda, A. V. Manohar, H. Murayama, and O. Telem, *Axion strings are superconducting*, *JHEP* **06** (2021) 052 [[arXiv:2010.02763 \[hep-ph\]](#)].
- [12] Y. Abe, Y. Hamada, and K. Yoshioka, *Electroweak axion string and superconductivity*, *JHEP* **06** (2021) 172 [[arXiv:2010.02834 \[hep-ph\]](#)].
- [13] P. Agrawal, A. Hook, J. Huang, and G. Marques-Tavares, *Axion string signatures: a cosmological plasma collider*, *JHEP* **01** (2022) 103 [[arXiv:2010.15848 \[hep-ph\]](#)].
- [14] L. M. A. Bettencourt and T. W. B. Kibble, *Nonintercommuting configurations in the collisions of type I $U(1)$ cosmic strings*, *Phys. Lett. B* **332** (1994) 297–304 [[arXiv:hep-ph/9405221](#)].
- [15] L. M. A. Bettencourt, P. Laguna, and R. A. Matzner, *Nonintercommuting cosmic strings*, *Phys. Rev. Lett.* **78** (1997) 2066–2069 [[arXiv:hep-ph/9612350](#)].
- [16] E. J. Copeland, T. W. B. Kibble, and D. A. Steer, *Collisions of strings with Y junctions*, *Phys. Rev. Lett.* **97** (2006) 021602 [[arXiv:hep-th/0601153](#)].
- [17] E. J. Copeland, T. W. B. Kibble, and D. A. Steer, *Constraints on string networks with junctions*, *Phys. Rev. D* **75** (2007) 065024 [[arXiv:hep-th/0611243](#)].

- [18] P. Salmi, A. Achúcarro, E. J. Copeland, T. W. B. Kibble, R. de Putter, and D. A. Steer, *Kinematic constraints on formation of bound states of cosmic strings: Field theoretical approach*, *Phys. Rev. D* **77** (2008) 041701 [[arXiv:0712.1204 \[hep-th\]](#)].
- [19] N. Bevis and P. M. Saffin, *Cosmic string Y-junctions: A Comparison between field theoretic and Nambu-Goto dynamics*, *Phys. Rev. D* **78** (2008) 023503 [[arXiv:0804.0200 \[hep-th\]](#)].
- [20] N. Bevis, E. J. Copeland, P.-Y. Martin, G. Niz, A. Pourtsidou, P. M. Saffin, and D. A. Steer, *Evolution and stability of cosmic string loops with Y-junctions*, *Phys. Rev. D* **80** (2009) 125030 [[arXiv:0904.2127 \[hep-th\]](#)].
- [21] T. Hiramatsu, M. Eto, K. Kamada, T. Kobayashi, and Y. Ookouchi, *Instability of colliding metastable strings*, *JHEP* **01** (2014) 165 [[arXiv:1304.0623 \[hep-ph\]](#)].
- [22] T. Hiramatsu, Y. Sendouda, K. Takahashi, D. Yamauchi, and C.-M. Yoo, *Type-I cosmic string network*, *Phys. Rev. D* **88** no. 8, (2013) 085021 [[arXiv:1307.0308 \[astro-ph.CO\]](#)].
- [23] C. J. A. P. Martins, P. Peter, I. Y. Rybak, and E. P. S. Shellard, *Generalized velocity-dependent one-scale model for current-carrying strings*, *Phys. Rev. D* **103** no. 4, (2021) 043538 [[arXiv:2011.09700 \[astro-ph.CO\]](#)].
- [24] C. J. A. P. Martins, P. Peter, I. Y. Rybak, and E. P. S. Shellard, *Charge-velocity-dependent one-scale linear model*, *Phys. Rev. D* **104** no. 10, (2021) 103506 [[arXiv:2108.03147 \[astro-ph.CO\]](#)].
- [25] E. Babichev and V. Dokuchaev, *Gravitational radiation from chiral string cusps*, *Phys. Rev. D* **67** (2003) 125016 [[arXiv:astro-ph/0303659](#)].
- [26] P. Auclair, S. Blasi, V. Brdar, and K. Schmitz, *Gravitational Waves from Current-Carrying Cosmic Strings*, [arXiv:2207.03510 \[astro-ph.CO\]](#).
- [27] I. Y. Rybak and L. Sousa, *Emission of gravitational waves by superconducting cosmic strings*, [arXiv:2209.01068 \[gr-qc\]](#).
- [28] R. L. Davis and E. P. S. Shellard, *COSMIC VORTONS*, *Nucl. Phys. B* **323** (1989) 209–224.
- [29] R. L. Davis and E. P. S. Shellard, *The Physics of Vortex Superconductivity. 2*, *Phys. Lett. B* **209** (1988) 485–490.
- [30] R. H. Brandenberger, B. Carter, A.-C. Davis, and M. Trodden, *Cosmic vortons and particle physics constraints*, *Phys. Rev. D* **54** (1996) 6059–6071 [[arXiv:hep-ph/9605382](#)].
- [31] C. J. A. P. Martins and E. P. S. Shellard, *Limits on cosmic chiral vortons*, *Phys. Lett. B* **445** (1998) 43–51 [[arXiv:hep-ph/9806480](#)].

- [32] C. J. A. P. Martins and E. P. S. Shellard, *Vorton formation*, [Phys. Rev. D **57** \(1998\) 7155–7176](#) [[arXiv:hep-ph/9804378](#)].
- [33] A. Cordero-Cid, X. Martin, and P. Peter, *Current carrying cosmic string loops 3-D simulation: Towards a reduction of the vorton excess problem*, [Phys. Rev. D **65** \(2002\) 083522](#) [[arXiv:hep-ph/0201097](#)].
- [34] P. Peter and C. Ringeval, *A Boltzmann treatment for the vorton excess problem*, [JCAP **05** \(2013\) 005](#) [[arXiv:1302.0953](#) [[astro-ph.CO](#)]].
- [35] P. Auclair, P. Peter, C. Ringeval, and D. Steer, *Irreducible cosmic production of relic vortons*, [JCAP **03** \(2021\) 098](#) [[arXiv:2010.04620](#) [[astro-ph.CO](#)]].
- [36] M. Ibe, S. Kobayashi, Y. Nakayama, and S. Shirai, *On Stability of Fermionic Superconducting Current in Cosmic String*, [JHEP **05** \(2021\) 217](#) [[arXiv:2102.05412](#) [[hep-ph](#)]].
- [37] J. E. Kim, *Weak Interaction Singlet and Strong CP Invariance*, [Phys. Rev. Lett. **43** \(1979\) 103](#).
- [38] M. A. Shifman, A. I. Vainshtein, and V. I. Zakharov, *Can Confinement Ensure Natural CP Invariance of Strong Interactions?*, [Nucl. Phys. B **166** \(1980\) 493–506](#).
- [39] A. R. Zhitnitsky, *On Possible Suppression of the Axion Hadron Interactions. (In Russian)*, [Sov. J. Nucl. Phys. **31** \(1980\) 260](#).
- [40] M. Dine, W. Fischler, and M. Srednicki, *A Simple Solution to the Strong CP Problem with a Harmless Axion*, [Phys. Lett. B **104** \(1981\) 199–202](#).
- [41] M. Eto, M. Kurachi, and M. Nitta, *Constraints on two Higgs doublet models from domain walls*, [Phys. Lett. B **785** \(2018\) 447–453](#) [[arXiv:1803.04662](#) [[hep-ph](#)]].
- [42] M. Eto, M. Kurachi, and M. Nitta, *Non-Abelian strings and domain walls in two Higgs doublet models*, [JHEP **08** \(2018\) 195](#) [[arXiv:1805.07015](#) [[hep-ph](#)]].
- [43] M. Eto, Y. Hamada, and M. Nitta, *Stable Z-strings with topological polarization in two Higgs doublet model*, [JHEP **02** \(2022\) 099](#) [[arXiv:2111.13345](#) [[hep-ph](#)]].
- [44] Y. Lemperiere and E. P. S. Shellard, *Vorton existence and stability*, [Phys. Rev. Lett. **91** \(2003\) 141601](#) [[arXiv:hep-ph/0305156](#)].
- [45] R. A. Battye and P. M. Sutcliffe, *Vorton construction and dynamics*, [Nucl. Phys. B **814** \(2009\) 180–194](#) [[arXiv:0812.3239](#) [[hep-th](#)]].
- [46] E. Radu and M. S. Volkov, *Existence of stationary, non-radiating ring solitons in field theory: knots and vortons*, [Phys. Rept. **468** \(2008\) 101–151](#) [[arXiv:0804.1357](#) [[hep-th](#)]].
- [47] J. Garaud, E. Radu, and M. S. Volkov, *Stable Cosmic Vortons*, [Phys. Rev. Lett. **111** \(2013\) 171602](#) [[arXiv:1303.3044](#) [[hep-th](#)]].

- [48] R. A. Battye and S. J. Cotterill, *Stable Cosmic Vortons in Bosonic Field Theory*, *Phys. Rev. Lett.* **127** no. 24, (2021) 241601 [[arXiv:2111.07822 \[hep-ph\]](#)].
- [49] R. A. Battye, S. J. Cotterill, and J. A. Pearson, *A detailed study of the stability of vortons*, *JHEP* **04** (2022) 005 [[arXiv:2112.08066 \[hep-ph\]](#)].
- [50] P. Peter, *Influence of the electric coupling strength in current carrying cosmic strings*, *Phys. Rev. D* **46** (1992) 3335–3349.
- [51] M. Bando, T. Kugo, T. Noguchi, and K. Yoshioka, *Brane fluctuation and suppression of Kaluza-Klein mode couplings*, *Phys. Rev. Lett.* **83** (1999) 3601–3604 [[arXiv:hep-ph/9906549](#)].
- [52] T. Kugo and K. Yoshioka, *Probing extra dimensions using Nambu-Goldstone bosons*, *Nucl. Phys. B* **594** (2001) 301–328 [[arXiv:hep-ph/9912496](#)].